Scientific report; WR 99 - 01

KNMI

Enhancement of Solar and Ultraviolet Surface Irradiance Under Partial Cloudy Conditions

Serdal Tunc

De Bilt, 1999

Koninklijk Nederlands Meteorologisch Instituut

Scientific report = wetenschappelijk rapport; WR 99 - 01

De Bilt, 1999

PO Box 201
3730 AE De Bilt
Wilhelminalaan 10
De Bilt
The Netherlands
Telephone + 31(0)30-220 69 11
Telefax + 31 (0)30-221 04 07

Author: Serdal Tunc
Institute of Marine and Atmospheric Research, University of Utrecht

UDC: 551.521.1
551.521.17
(043.3)

ISSN: 0169-1561

ISBN: 90-369-2156-2

Enhancement of Solar and Ultraviolet Surface Irradiance Under Partial Cloudy Conditions

Serdal Tunc

Graduation research project performed at

The Royal Netherlands Meteorological Institute (KNMI)

Division of Climate Research and Seismology

Section of Atmospheric Composition

De Bilt, The Netherlands

February, 1999

Institute of Marine and Atmospheric Research (IMAU)

University of Utrecht

Princetonplein 5, 3584 CC Utrecht, The Netherlands

Abstract

Clouds are important for the transfer of solar radiation to the Earth's surface. In this study, the enhancements of the global irradiance due to the contributions of the direct and diffuse components of the solar radiation are investigated using the 10 seconds irradiance measurements of De Bilt (52.100 N, -5.183) during 1995 and 1996, which consist of the global, direct and diffuse surface irradiance of the total solar spectrum (300-3000 nm) and the global and direct surface irradiance of the UV-A (367 nm with FWHM=10 nm) and UV-B (306 nm with FWHM=3 nm) spectral regions. The dataset is completed with hourly standard meteorological observations, including cloud coverage, cloud base height, cloud type, horizontal visibility etc. With use of a constructed cloud-free reference as a function of solar zenith angle, enhancements of 73 %, 50 % and 60 % are calculated for the total solar spectrum, UV-A and UV-B, respectively.

Most of the enhancements are observed when cumulus-like clouds are present. We find that enhancements are most likely within the cloud coverage (N) and the cloud base height (h) combinations: $0.125<N\leq0.625$ with $100\ m\leq h\leq900\ m$ and $0.625<N\leq1$ with $900\ m<h\leq1500\ m$. We show under what conditions the highest irradiances are found in terms of cloud coverage, cloud base height, cloud type and solar zenith angle.

Two models are constructed in which cloud coverage is derived in 10 minute intervals from the irradiance data. One model uses both direct and global irradiance of the total solar spectrum and the other uses only the global irradiance of the total solar spectrum. The derived cloud coverage data are succesfully compared with the hourly available observations of cloud coverage.

Contents

	Page
Abstract	
1. Introduction	*1*
2. Data	*4*
2.1. Measurement Site	*4*
2.2. Instrumentation	*5*
2.3. Synoptic data	*10*
3. Data analysis	*12*
3.1. Cloud-free reference	*12*
3.2. Radiation amplification factor (RAF)	*13*
3.3. Enhancements over cloud-free reference	*16*
4. A simple model for cloud coverage (N)	*22*
4.1. Theory	*22*
4.2. Model 1	*25*
4.3. Model 2	*26*
4.4. An empirical method for cloud coverage	*27*
4.5. Cloud Transmission	*28*
5. Case Studies	*29*
5.1. "16 July 1996"	*30*
5.2. Other days	*34*
6. Conclusions	*38*
7. Acknowledgements	*40*
8. References	*41*
Appendices	*43*
Appendix A, • R^2	*43*
• *Estimated standard error of the dependent variable (y):* S_y	*43*
Appendix B, • *Variation in the Earth-Sun distance*	*44*
• *The solar zenith angle (SZA)*	*44*

1. Introduction

Clouds play an important role in the transfer of solar radiation to the Earth's surface. Clouds usually reduce the solar radiation at the Earth's surface. Clouds can also cause an enhancement of the surface irradiance with respect to cloud-free values. Clouds are very difficult to model because of their three-dimensional structure and complex morphology. The increase of the irradiance at the Earth's surface under partial cloudiness is attributed to the reflections from the sides of clouds *(Laird and Harshvardhan, 1997). Segal and Davis (1991)* called these CSIR (Cumulus Solar Irradiance Reflection) events. The occurrence of surface irradiances higher than the cloud-free value has in general short duration. A maximum observed duration of about 30 minutes is detected. Both duration and magnitude of these events depend on the type of cloud and cloudiness, the position of the Sun and the movement of the clouds. This enhancement is less relevant for the climatological mean values, because of its short duration.

The distribution of solar radiation emitted by the Sun as a function of the wavelength incident on the top of the atmosphere is called the solar spectrum. This shortwave radiation can be subdivided into (Ultraviolet) UV, visible (VIS) and near infrared radiation (NIR). The UV region spans the 10 to 400 nm wavelength range and contains less than 9 % of the energy in the total solar spectrum (TSS). This wavelength range can be subdivided into extreme UV (EUV, 10-120 nm), far UV (120-200 nm), UV-C (200-280 nm), UV-B[1] (280-320 nm), UV-A (315-400 nm). These are highly variable at the Earth's surface due to geometric factors such as the position of the Earth relative to the Sun, Earth's rotation around its own axis, the latitudinal variations of the angle at which sunlight enters the Earth's atmosphere and the changes in the atmospheric composition and the surface reflectivity. Wavelengths shorter than about 280 nm are absorbed almost completely by the atmosphere. The effective UV radiation for the biosphere is therefore finite and is a combination of UV-A and UV-B ranges, which spans from 280 up to 400 nm.

Absorption of UV is one of the obstacles that should be excluded before studying the influence of clouds on surface UV irradiance (*Madronich et al, 1995, Bordewijk et al, 1995, Frederick and Snell, 1990*). Extratropical ozone depletion and expected increase in UV radiation at the Earth's surface may influence the biosphere. Present datasets of surface UV with a resolution of 10 minutes are available for assessing these effects. *Bodeker and McKenzie (1996)* have developed a semi-empirical algorithm, making use of readily available meteorological variables and total column ozone, for inferring the historical UV levels at a particular location, including cloud cover effects. Their algorithm makes use of measured

[1]In some literature slightly different ranges of UV are defined, such as UV-B ranging from 280 upto 320 nm or from 290 upto 320 nm.

broadband irradiance and cloud-free erythemal and broadband irradiances calculated with statistical derivation from measured data and output from a surface spectral irradiance model.

Air pollutants have also an important influence on the surface irradiances. Because of the increase in industrialization, emission of pollutants in the atmosphere has been increased in the last century, especially in Western Europe. This can affect the UV radiation on the Earth's surface with a reduction in the intensity (*Liu et al., 1991*) and a relative increase in diffuse radiation. *Krotkov et al. (1998)* has used satellite data to estimate the UV irradiance in the presence of tropospheric aerosols and has concluded that a reduction of errors in satellite estimation of UV is strongly dependent on attenuation of UV by aerosols. The sulfate aerosol haze observed in urban and rural areas are increased with industrialization and causes substantial reduction of surface UV irradiance. *Jianzhong and Guicherit* showed that near the Earth's surface, in non-urban polluted regions, an increase of tropospheric pollution, which occurred over the last 50-100 years, has cancelled the effect of an increase of UV-B radiation due to stratospheric ozone depletion that has occurred since the late 1970s. If the interest in UV measurements is confined to ozone variations only, and if significant amounts of pollutant gases and aerosols are present, they will act to reduce the surface UV radiation more than that for ozone alone (*Deluisi, 1997*). In this study, the atmospheric composition is an important factor, because these elements of the atmosphere are variable in time. Differences between a partial cloudy day and a cloud-free sky are affected by those conditions. It follows that the winds of a certain direction can have also an effect on the surface irradiances, especially South and South-Eastern winds transport many air pollutants in the direction of The Netherlands where the measurements of this study are made. However, a Western wind, advects typically maritime aerosols effectively in the direction of De Bilt.

In this study, we investigate the effects of the partial cloudiness on the total solar spectrum (TSS), UV-A and UV-B irradiances at the Earth's surface. For this purpose, we have used the 10 seconds instantaneous measurements made at KNMI (Royal Netherlands Meteorological Institute) in De Bilt. There are measurements available of global (vertical component of the irradiance, which is equal to the sum of diffuse and direct irradiances), direct and diffuse irradiances for TSS, UV-A and UV-B. Enhancements of global irradiance for De Bilt are computed with several methods. One of the methods is to compare the irradiance measurements of a cloud-free day with the same day in another year or when it was partial cloudy. Another method is to construct a cloud-free reference using the irradiance measurements of the cloud-free days. Absorption of UV radiation by ozone forms a problem by constructing the cloud-free reference for the UV range. We used a correction method based on a so-called radiation amplification factor (*RAF*), to filter out the influence of absorption of UV-B radiation by ozone.

Enhancements and the duration of enhancements are computed for all spectral ranges and are subdivided in three categories considering the instrumental errors, standard error of the cloud-free reference, and the values of direct irradiance. The enhancements are studied in dependence of solar zenith angle, measurement frequency and averaging periods for all

spectral ranges. The relationship between the clouds (cloud coverage, cloud type and cloud base height) and the enhancements is explored with hourly synoptic reports. For higher time resolution of cloud coverage, a model is needed. There are two models developed to compute cloud coverage for every 10 minutes using the irradiance data. Other synoptic parameters such as wind speed and wind direction are related to the enhancements. In addition, cloud transmissions of the different spectral ranges are related to the enhancements.

In Chapter 2 we describe the location of the measurements and the instrument properties including the error analysis and the uncertainties in the measurements. In this chapter we discuss also hourly synoptic reports that consist of observations of cloud types, height, layers and coverage, horizontal visibility, relative humidity, temperatur etc. Radiosonde data that consist of the vertical distribution of temperature, relative humidity, wind speed and wind direction, are visualized.

Construction of the cloud-free references of the global irradiance of TSS, UV-A and UV-B, and the correction method for the absorption of UV-B by ozone is described in Chapter 3. Also, the enhancements over the cloud-free reference is given in this chapter.

A simple model for cloud coverage is described in Chapter 4. Two types of models are developed: Model 1 and Model 2. The results of these models are compared with an empirical method for cloud coverage. With some approximations, cloud transmission is estimated.

In Chapter 5, we select some days for case studies, exhibiting strong and long enhancements. Enhancements on these days are studied using methods explained in previous chapters. Model 1, Model 2 and the cloud transmission estimation method are applied on these days and related to the enhancements in global irradiances.

In Chapter 6, we summarize our conclusions.

2. Data

2.1. Measurement Site

The measurements are made in De Bilt (52.100 N, -5.183 W). The instruments are mounted on top of a container on the roof at the southern end of a four-storey building at KNMI. The horizon is almost clear, except for a satellite dish on the adjacent roof at very low elevation to the north-west, a tall brick tower to the north, with on top a precipitation radar, and a few isolated antenna masts. Apart from a few houses close by, the institute is surrounded by parkland with trees, meadow, and gardens. The city of Utrecht lies in the western and southern quadrants at a distance of about 5 km. To the north is the village of Bilthoven at about 1km. In the north-east quadrant the land is forested. The village of Zeist is at a distance of 5 km to the south-east, with forest beyond.

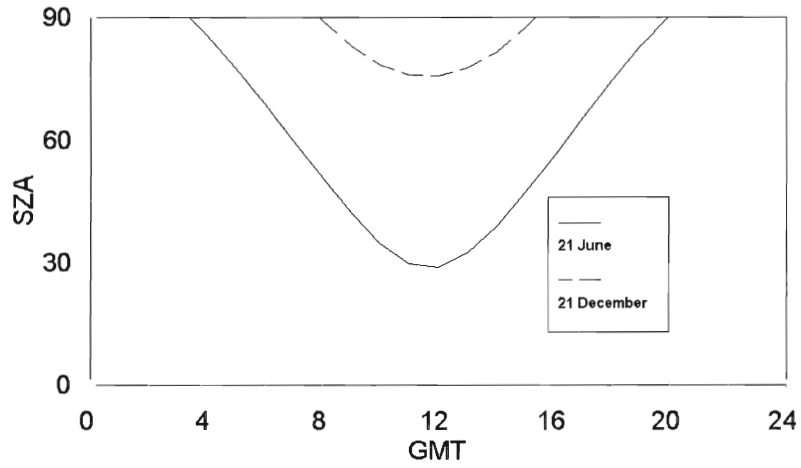

Figure 2.1. *Solar zenith angles (SZA) in De Bilt for 21 June and 21 December.*

The solar zenith angles (SZA) in De Bilt for 21 June and 21 December are given in Figure 2.1 as a function of GMT (Greenwich Mean Time) where the domain also includes the time when the Sun is already down. Sunset and sunrise occur at a solar zenith angle of 90^0. The midday value in De Bilt is about 30^0 and 75^0 at 21 June and 21 December, respectively. The calculation of SZA is described in Appendix B.

2.2. Instrumentation

Measurements of global, direct and diffuse irradiance are available for total solar spectrum (TSS). For the UV-A and UV-B region, we have only the global and direct irradiance measurements. The data is sampled in 10 seconds time intervals in 1995 and 1996, and in 10 minutes interval since 1997. For each irradiance measurement, the air temperature around the instruments is recorded. In this study we use only the data of 1995 and 1996 and focus on the period of May-August.

The instruments used to obtain the irradiance data are the narrow-band UV-meters and the pyranometers. Pyranometers measure the irradiance between 300 nm and 3000 nm. Pyranometers are used to measure the global irradiance, i.e. the direct and diffuse components of the irradiance. The scattered component of the global irradiance is measured by obscuring the Sun's disc with a shadow band. Direct irradiance measurements are made by following the Sun and excluding the diffuse irradiance. This instrument is named a "pyrheliometer". Instrumental error is about 3 % for pyranometers and pyrheliometers, and about 6 % for the narrow band UV-meters *(Kuik, 1997)*.

The sum of the diffuse and direct irradiance measurements of the total solar spectrum is compared with the measurements of the other independent instrument, which measures the global irradiance of the total solar spectrum. From this comparison, it is concluded that this sum is not precisely equal to the global irradiance. The difference is attributed to instruments properties. Global irradiance values are always higher than the sum of diffuse and direct irradiance values. The calculated mean difference is 2 % of the measured global irradiance. However, this value increases for increasing solar zenith angle. On 25 July 1995 this difference reaches a value of 4.5 % at a solar zenith angle of 62 ^{0}.

The stability of the instruments is important for comparing the irradiance measurements of different days. In order to check a possible drift in some of the instruments we compare data of two cloud-free days, one day in 1995 and one day in 1996. In Figure 2.2, data of two cloud-free days are plotted. These two days are 25 July 1995 and 20 July 1996. Only the measurements between 8 and 16 GMT are included. There are distinct differences between the irradiance measurements of these days. Mean cloud coverage on 25 July 1995 is about 2 % and on 20 July 1996 about 25 %. According to synoptic measurements cirrus clouds were present in the morning, later in the afternoon cumulus clouds were observed on 20 July 1996, and therefore the irradiance values in the afternoon of 20 July 1996 are excluded. Attenuation of the solar radiation by the cumulus clouds in the afternoon causes fluctuations around noon on 20 July 1996. Global

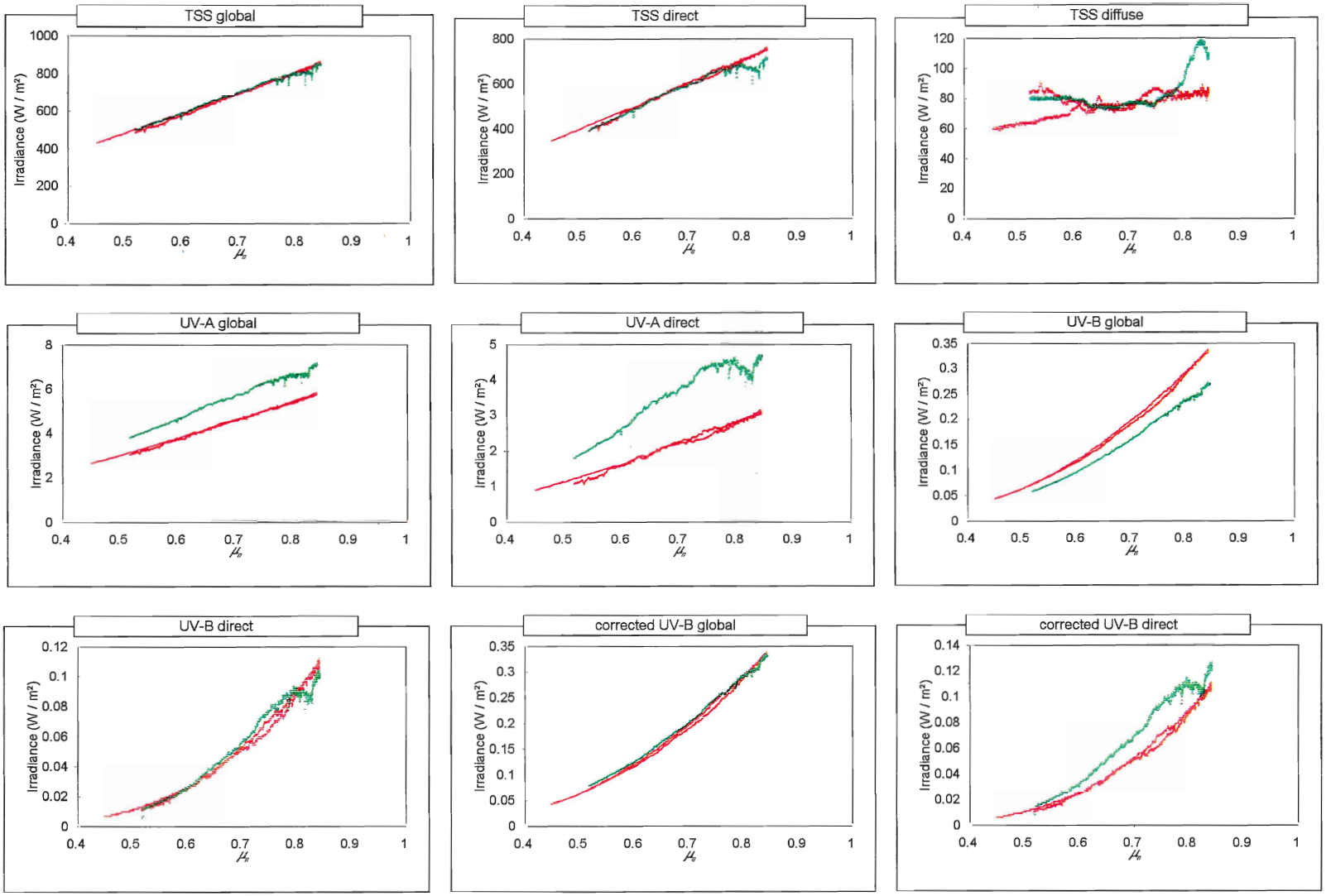

Figure 2.2. *Comparison of cloud-free irradiance measurements of 25 July 1995 (red lines, 293 DU) with 20 July 1996 (green lines, 323 DU). Only the measurements between 8 and 16 GMT are plotted as a function of μ_0 (cosine of SZA). Corrected UV-B values are obtained with the RAF correction method where the ozone column amount of 25 July 1995 is used as reference. These days are selected as cloud-free days, nevertheless some clouds were observed. In the afternoon cumulus clouds were observed on 20 July 1996, therefore the irradiance values after 12 GMT are not plotted. On 25 July 1995 thin cirrus clouds were observed in the morning hours.*

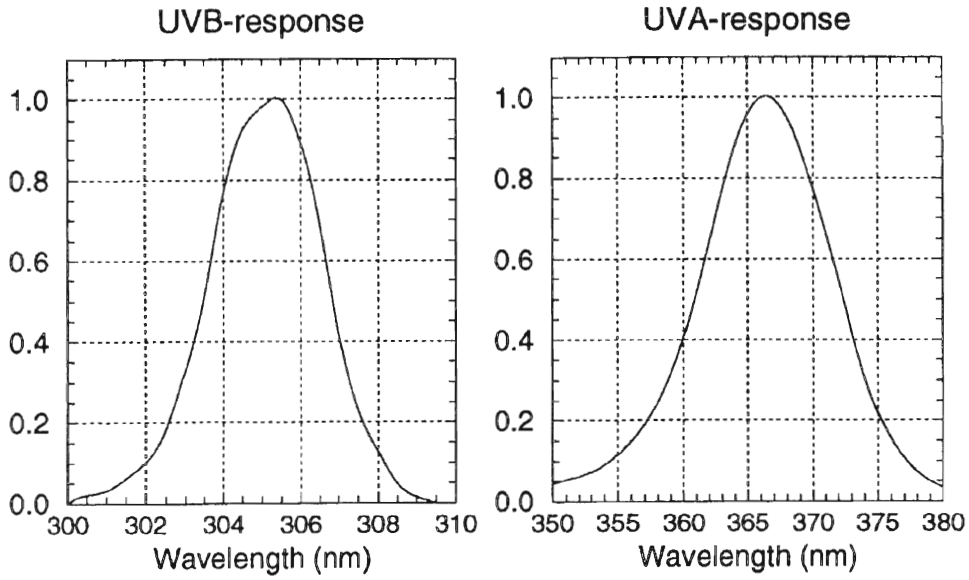

Figure 2.3. *Spectral responses of the UV-B and UV-A sensors. The UV sensors manufactured by Kipp & Zonen are CUVA1/CUVB1 type for the measurements of global and diffuse components, and CUVA2/CUVB2 type for the measurements of the direct component.*

and direct measurements of TSS of both days appear comparable. The mean absolute difference is 11.4 W/m^2 (1.7% with respect to 25 July 1995). Diffuse irradiance of TSS is higher on 20 July 1996 (Figure 2.2) around noon corresponding with increasing cloud coverage in the afternoon.

Narrow-band UV-meters are characterized by the filters built inside the instruments, which determine the spectral response. In the UV range, measurements of the direct component of the global irradiance are made in the same way as for the TSS. The UV-B meters are operating around 306 nm and the filter has a bandwidth of 3 nm (Full-width half maximum: FWHM). UV-A meters are operating around 367 nm and have a bandwidth of 10 nm (FWHM). Spectral responses of the instruments are shown in Figure 2.3 (measured by *Kipp & Zonen*).

In the UV-A range there are distinct differences in the global and the direct components. Mean differences are +24 % and +61 % for the global and direct components, respectively, with the higher values in 1996. In the UV-B range, mean differences are +18 % and +7 % for the global and direct components, respectively, with the higher values in 1995. The big difference in the UV-A may be attributed to the aerosol characteristics. The wind direction on 25 July 1995 was East, North-East and on 20 July 1996 it was West, South-West. Because of the industrial emissions in Western Europe, easterly winds bring air pollutants above De Bilt while the westerly winds bring cleaner air. Also, the wind speed was higher on 20 July 1996. Other synoptic parameters such as higher horizontal visibility and lower relative humidity on 20 July 1996 show that these two days have rather different air contents. In the UV-B range the values of the global irradiance on 25 July 1995 (293 DU) are higher than on 20 July 1996 (323 DU). UV-B radiation is very sensitive to the ozone column amounts. 34 DU difference in ozone column amount causes

that the UV-B irradiance is higher on 25 July 1995. In Chapter 3 a method is described (The Radiation Amplification Factor (*RAF*) correction method) to filter out the influence of the total ozone column. With this method, it is possible to shift the measured UV-B irradiance with a certain ozone column amount to a reference ozone column amount. Figure 2.3 shows the corrected global UV-B irradiance where the reference ozone column amount is that of 25 July 1995. Mean difference of the plotted global irradiance values of these two days is decreased from +18 % to +3 % and the mean values of 20 July 1996 lie slightly above that of 25 July 1995 corresponding with possible lower aerosol amount on 20 July 1996. If the aerosol content would explain the difference observed between both days, this would imply that aerosols attenuate more effectively the UV-A irradiance than the UV-B irradiance considering the higher difference in the UV-A and the lower difference in the corrected UV-B irradiance.

The elliptical orbit of the Earth with the Sun at one of the foci, causes variations in the Earth-Sun distance. The calculation of Earth-Sun distance is described in Appendix B. Earth-Sun distance varies about 1 % in the summer months. The influence of the variation in the Earth-Sun distance is relatively low and is neglected in further calculations.

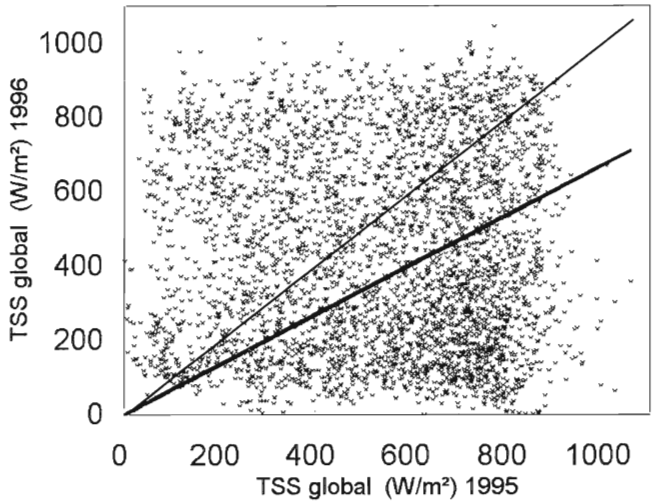

Figure 2.4. *Global irradiance of TSS in 1996 against global irradiance of TSS in 1995. 10 minutes averaged values in May, June, July and August between 8 and 16 GMT are used.*

To explore the year-to-year variations of the measurements the global irradiance values of TSS in 1996 are plotted against the global irradiance values of TSS in 1995 (Figure 2.4). Most of the plotted points are collected below the thin line, which divides the higher or lower irradiance values versus the other year. According to the synoptic data 1995 was about 12 % sunnier than 1996. That is to observe in Figure 2.4 with more points below the thin line and a best line through the points passing the origin with a slope of 0.7.

In Figure 2.5 the available irradiance data are plotted against the global irradiance of TSS. There seems to be a linear relation between diffuse irradiance and global irradiance of TSS for lower values of them (Figure 2.5b). These are the moments when the diffuse irradiance is equal to the global irradiance, meaning that direct irradiance value is zero (Figure 2.5a). There are no diffuse irradiance values lower than 80 W/m^2 between 8 and 16 GMT.

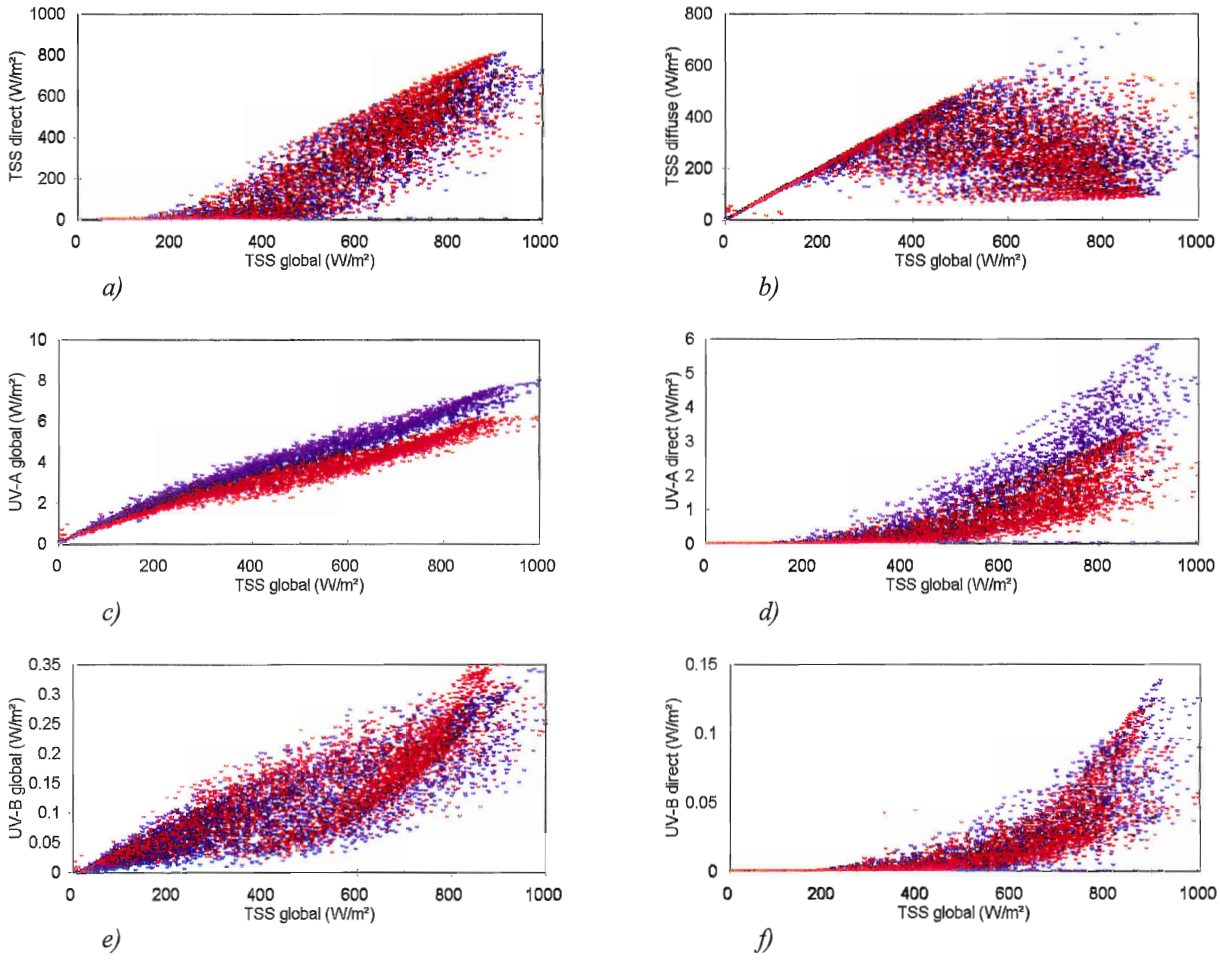

Figure 2.5. *Plots of available irradiance data against global irradiance of TSS. 10 minutes averaged values in May, June, July and August between 8 and 16 GMT in 1995 (red dots) and 1996(blue dots) are used. a) TSS direct, b) TSS diffuse, c) UV-A global, d) UV-A direct, e) UV-B global, f) UV-B direct.*

The UV-A instruments measured higher values in 1996 than in 1995; difference of about 2 and 3 W/m^2 is found by global and direct irradiance measurements, respectively for highest irradiance values (Figure 2.5c,d). The global irradiance of UV-B is slightly higher in 1995 than in 1996 (Figure 2.5e). From the direct irradiance measurements of UV-B, it is not obvious whether

the values of 1995 or 1996 are higher. These shifts in the UV irradiance measurements are the reason to get in touch with the manufacturer of the UV meters (*Kipp & Zonen*, The Netherlands). They checked the irradiance records of the UV meters and concluded that the instruments indeed have changed since 1995. According to the manufacturer, a possible explanation is a transmission change of the diffuser material of the instruments. In this report, we will use only absolute UV measurements of 1995. The UV measurements of 1996 are only used in a relative way. In future, it may be considered to use the pyranometer and pyrheliometer data to correct the UV data of 1996.

2.3. Synoptic Data

To compare the radiation data with clouds, synoptic data are included in our dataset. This data has a resolution of one hour. The synoptic data contains total cloud coverage (in octa, 1 octa = 12.5 % of the sky is covered by clouds), and cloud coverage, height, kind of the lowest (first), second, third and fourth cloud layers (Figure 2.6). Cloud observations are made by a meteorologist who makes visual observations 10 minutes before every observation hour. The observer looks at the sky and determines approximately the cloud coverage of the cloud layers, height of the bottom of each cloud layer from the ground and the kind of clouds. For this study, cloud data is most important part of the total synoptic data. The estimated error in cloud coverage is 1 octa. Beside cloud information, the synoptic dataset contains records of air temperature at 1.5 m altitude, relative humidity, air pressure at sea level and horizontal visibility.

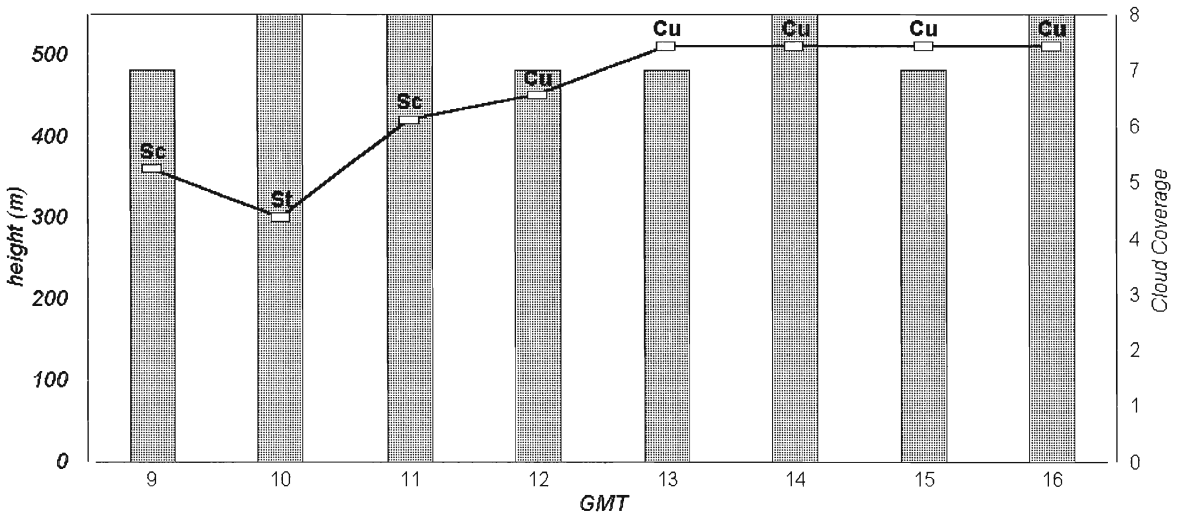

Figure 2.6. *Synoptic data of 25 July 1996. Cloud base heights (solid lines), Cloud types (on this day; Sc, St, Cu) and total cloud coverage (dotted bars).*

There are also 6-hourly radiosonde records available. Radiosonde records contain vertical profiles of pressure, temperature, dew-point temperature, relative humidity, wind direction and wind speed at all recorded altitudes (Figure 2.7).

There is also total ozone column data used in this study to attain the influence of the ozone column on the spectral distribution and the attenuation of the solar radiation by this molecule. For this purpose we have used the values of the ozone column in DU (Dobson Units) for every day at 12.00 GMT, as measured by a Brewer photospectrometer.

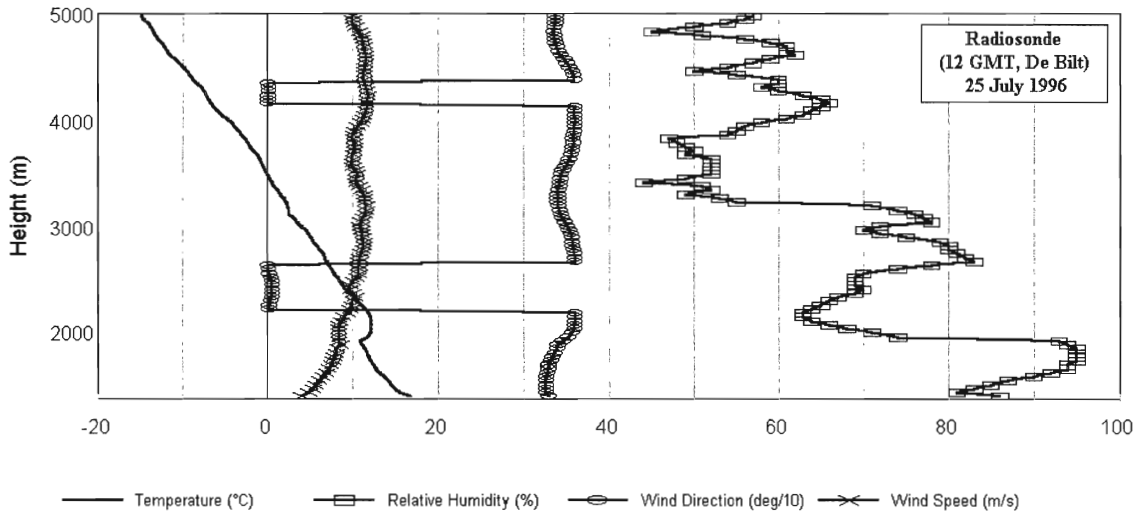

Figure 2.7. *Radiosonde data of 25 July 1996 on 12 GMT.*

A Brewer MK III spectroradiometer (#100) is operated on the site since 1994. Spectra of UV surface irradiance (290 - 365 nm) with 0.5 nm steps are collected routinely for about every 5 degrees change in solar zenith angle. Data of the narrow-band meters are regularly compared with the Brewer spectra and under various atmospheric conditions. During the years Brewer spectroradiometer has participated in several international intercomparisons and its calibrations are well confirmed *(Kuik, 1997)*.

3. Data Analysis

3.1. Cloud-Free Reference

The cloud-free reference is constructed using days that satisfy the cloud-free criterion. The most important criterion for a cloud-free day is that the curves of the global, diffuse and direct irradiance components of all the spectral ranges measured by the instruments have a smooth form. In our dataset that consist of about two years (1995 and 1996) we could find only three days (25 July 1995, 1 August 1995, 20 July 1996) that could represent a cloud-free day. All the selected days are in the summer. Only in the summer, the Sun rises enough to get the maximum irradiance values that are needed to construct a reference that spans all possible SZA. In Figure 3.2 the curves of 25 July of 1995 are a good example of a cloud-free day. Global irradiance shows a smooth course in TSS as well as in the UV-A and UV-B range. Diffuse irradiance is very low and almost constant between 8 and 15 GMT. It has relatively higher values only around 7 GMT when we also have decreasing values of direct and global irradiance. Fluctuations in irradiance measurements are caused by the cirrus clouds observed between 7 and 8 GMT in De Bilt. The decrease in the direct component is only partly compensated by the increase in the diffuse component of the global irradiance.

There are several methods to visualize the influence of the partial cloudiness on the irradiance values at the Earth's surface. One of them is to compare the irradiance measurements of a cloud-free day with the same day in another year. With this method, it is tried to compare the irradiance values for the same SZA. Figure 3.2 shows such an example for 25 July. In the next chapter, we explain the enhancements over the cloud-free measurements of 1996 that are observed around noon on this day. As explained above there were only three days available for De Bilt that satisfy the cloud-free reference. Thus, we can not study the other partial cloudy days with this method. To solve this problem, we can use the cloud-free reference equation, which is constructed with a polynomial fit of the irradiance measurements of those three cloud-free days. The global irradiance (E_{glb}) of the cloud-free days is plotted in Figure 3.1 for TSS, UV-A and UV-B range as a function of cosine of solar zenith angle (μ_0). With this method of visualizing the GMT dependence of the irradiance is replaced by μ_0. It is possible to make a third degrees polynomial fit through the origin. The third degrees polynomial function through the origin has the following form,

$$E_{glb} = a_1 \mu_0 + a_2 \mu_0^{\,2} + a_3 \mu_0^{\,3} \qquad (3.1.1)$$

The fits are obtained with the least-squares method. The fits for TSS, UV-A and UV-B are shown in Figure 3.1. The coefficients a_1-a_3 are given in Table 3.1. The fit for the TSS seems to be a good approximation for the measurements on three days. Data of UV-A and UV-B of 1996 are not used in these plots because of the reasons explained in Chapter 2. In Figure 3.1b and 3.1c

differences between the two days in the UV region are obvious because of the different aerosol properties, ozone column amount and air molecules of the two cloud-free days in 1995. In the previous chapter (instrumentation) the possible causes of these differences are explained.

	a_1	a_2	a_3
TSS	481.32±20.86	1139.47±72.11	-649.44±59.66
UV-A	2.88±0.22	6.07±0.76	-2.10±0.63
UV-B	-0.0089±0.0151	-0.1031±0.0525	0.5949±0.0450
UV-B corrected	-0.0200.0.0090	-0.0220. ±0.312	0.5900±0.0250

Table 3.1. *Coefficients for the polynomial fits through the origin of TSS, UV-A, UV-B and UV-B corrected to 300 DU with RAF correction method.*

3.2. Radiation amplification Factor *(RAF)*

The points of UV-B are widely separated from each other (Figure 3.1c). This distribution is mostly caused by different ozone column amounts, which is an effective absorber of UV-B radiation. Given the higher ozone column amount of 1 August 1995 (317 DU) relative to 25 July 1995 (293 DU) the points of 1 August lie under the points of 25 July. The fit attained with these values of UV-B gives the fit in Figure 3.1c. Smaller R^2 (see Appendix A for the definition of R^2 and standard error) and the wide distribution of points in this figure shows that this fit is not a good approximation for the cloud-free reference of the UV-B irradiance. There must be a correction applied to filter out this effect. One possible correction method is that one of the dataset of a day with a certain ozone column density to be chosen as the reference measure or an arbitrary ozone column amount. After this choice, we use the radiation amplification factor (*RAF*) method to deduce the attenuation of the global, direct and diffuse irradiances of UV-B by ozone. The derivation of the equation of this method is as follows,

$$u = \int_{z1}^{z2} [O_3]dz \qquad (3.2.1)$$

u = Total ozone column from an altitude of $z1$ to $z2$ and O_3 is the ozone concentration (molecules/cm^2).

$$E_{dir} = \mu_0 S_0 e^{-(\sigma u + \tau_s)/\mu_0} \qquad (3.2.2)$$

E_{dir} = Direct component of the irradiance

S_0 = Solar Constant
σ = Effective ozone absorption cross section (cm^2/molecules)
τ_s = Vertical optical depth of the atmosphere

From equations 3.2.2 follows,

$$\frac{\partial E_{dir}}{\partial u} = -\frac{\sigma}{\mu_0} E_{dir} \tag{3.2.3}$$

RAF is defined as,

$$RAF = -\frac{\partial \ln E}{\partial \ln u} \tag{3.2.4}$$

For direct irradiances follows,

$$RAF_{dir} = \frac{\sigma u}{\mu_0} \tag{3.2.5}$$

With use of the radiative transfer model (Tropospheric Ultraviolet and Visible Radiation Model, TUV) of Madronich, we have calculated the following *RAF* values of the global irradiance for De Bilt with the spectral response, cosine response and bandwidth of the measured spectral range as input parameters.

2.60 for SZA $\geq 40^o$
$1.99/\mu_0$ for SZA $\leq 40^o$

For larger SZA (smaller μ_0), the path length of the solar beam in the atmosphere is longer and due to the Rayleigh scattering much of the radiation is diffuse. Therefore, the attenuation by ozone is higher for higher SZA and, thus, *RAF* values of direct irradiance are increasing with increasing SZA. This is confirmed by the *RAF* values that are acquired with the TUV model. For SZA $\geq 40^o$ the *RAF* values are assumed to be constant, because much of the UV-B irradiance is scattered and the reduction of UV-B irradiance by ozone is then independent of the SZA.

To apply the correction for days with different values of ozone column we integrate the *RAF* equation (3.2.4) from u values of day one (reference day) to day two. Subscripts 1 and 2 refer to the day number.

$$\int_{E_1}^{E_2} \partial \ln E = -RAF \int_{u1}^{u2} \partial \ln u \tag{3.2.6}$$

From the equation above follows,

$$\frac{E_2}{E_1} = \left(\frac{u_1}{u_2}\right)^{RAF} \tag{3.2.7}$$

The reference day is day one, which it is here due to our choice, a day with a total ozone column of 300 DU. Global UV-B irradiances corrected with *RAF* values acquired with TUV model are plotted in Figure 3.1.d. Decrease in standard error of the irradiance and increase in R^2 shows the improvement of the fit of the cloud-free reference. The irradiance plots of the two days are still obvious most likely because of different aerosol and air molecules on these days. Exclusion of aerosol effects is complex and we are going to use the fit shown in Figure 3.1.d as the cloud-free reference for the UV-B range.

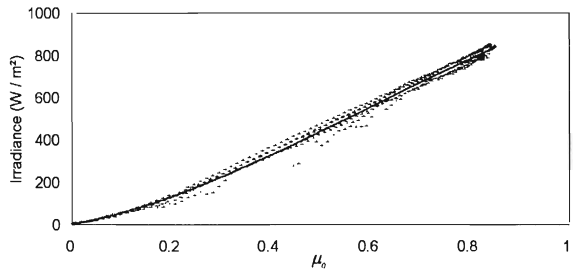

a) Standard error of irradiance =18, R^2 =0.996

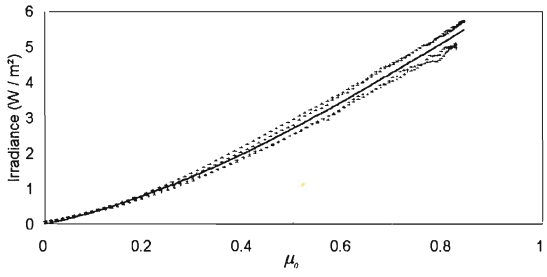

b) Standard error of irradiance =0.2, R^2 =0.989

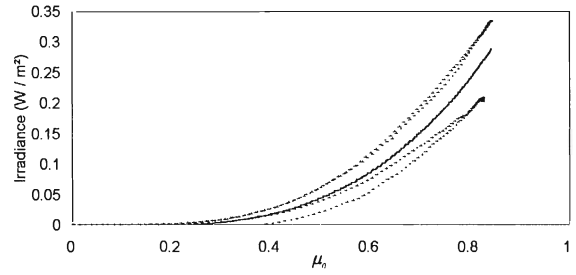

c) Standard error of irradiance = 0.03, R^2 =0.926

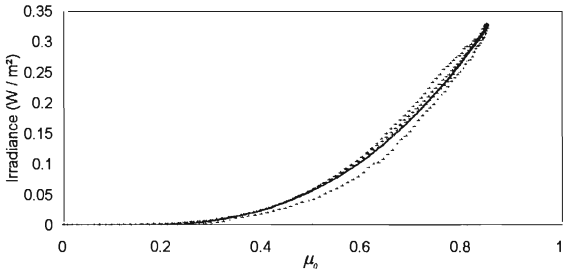

d) Standard error of irradiance = 0.01, R^2 =0.996

Figure 3.1. *Plots (dots) and 3. degrees polynomial fits (solid lines) of the global irradiances* ($E_{glb}=a_1\mu_0+ a_2\mu_0+a_3\mu_0$) *on cloud-free days. a) TSS, b) UV-A, c) UV-B, d) UV-B corrected to 300 DU. In the UV range the data of 1996 is not used as explained in Chapter 2.2.*

3.3. Enhancement over cloud-free reference

Enhancement over cloud-free reference is defined as,

$$\varepsilon = \left(\frac{E^{*}_{\mathrm{glb}}}{E^{0}_{\mathrm{glb}}} - 1 \right) \times 100 \qquad (3.3.1)$$

Where ε is the enhancement over cloud-free reference in percent. E^{*}_{glb} and E^{0}_{glb} are the measured and cloud-free reference of the global irradiance, respectively. Only positive values of ε point to an enhancement over cloud-free reference.

One way to visualize ε is comparing the partial cloudy day measurements of a certain day of the year with the same day of another year when a cloud-free sky was observed. Plots of such days are shown in Figure 3.2 for direct, diffuse and global irradiances of TSS, and direct and global irradiances of UV-A and UV-B. On the cloud-free day (25 July 1995) direct irradiances in the whole spectral ranges (Figure 3.2d) are regular, i.e. there are less fluctuations than on the partial cloudy day (25 July 1996). Diffuse irradiance has lower values and less fluctuation on the cloud-free day than on the partial cloudy day (Figure 3.2c). Observed cumulus clouds on the partial cloudy day cause these fluctuations. ε of TSS is about 22 % at 13.24.30 GMT (hours. minutes. seconds) (Figure 3.2a) and 16 % at 13.24.30 GMT for UV-A (Figure 3.2e).

In Figure 3.2g, there seem to be no ε values present in the UV-B. The main reason of this is that the UV-B plots in Figure 3.2 are not corrected for different ozone column amounts, which are 293 DU and 370 DU for the cloud-free day and the partial cloudy day, respectively. As explained in the previous chapter ozone is an effective absorber of the UV-B radiation. If the ozone column amount on the partial cloudy day was the same as on the cloud-free day, the irradiance values of UV-B would be higher on the partial cloudy day which could result in a positive ε. For example, according to the *RAF* values that are computed with the TUV model, irradiance values of the partial cloudy day for SZA = 40^{0} must be multiplicated with 1.8. With the *RAF* method comparison of the measured UV-B irradiance at different ozone column amounts is possible. Later in this chapter, we show results of ε calculations corrected with the *RAF* correction method for UV-B.

The ε values discussed above could be calculated with use of the available cloud-free day irradiance measurements of the same day in another year. To compute the ε values of the other partial cloudy days in our dataset, equation 3.3.1 is applied to the global irradiance of TSS, UV-A and UV-B measurements with use of the third-degree polynomial fit (equation 3.1.1)

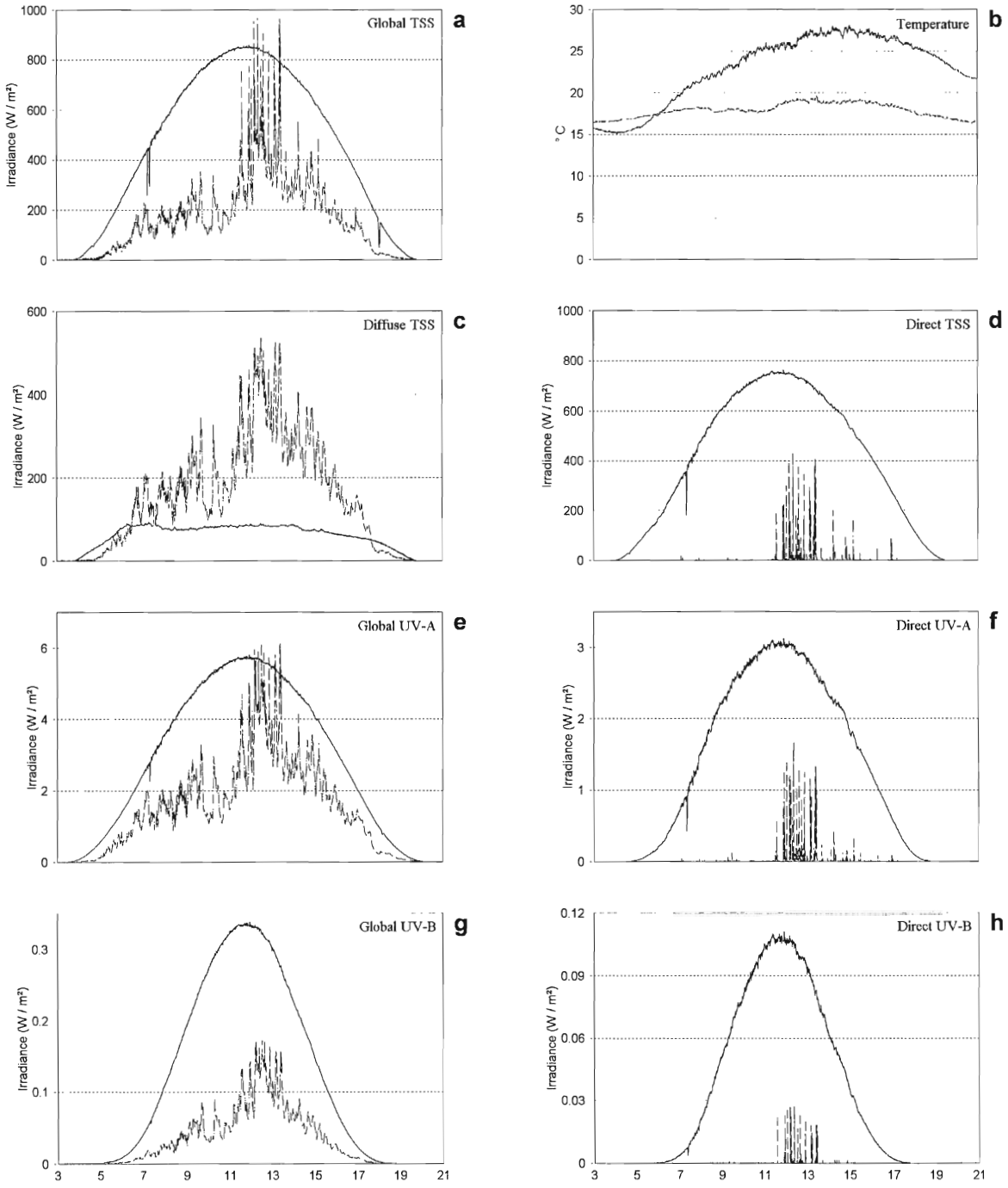

Figure 3.2. *Comparison of the irradiance measurements of 25 July 1995 (cloud-free day, solid lines) with 25 July 1996 (partial cloudy day, dashed lines). a) Global irradiance of TSS, b) Ambient temperature in De Bilt in ^{0}C, c) Diffuse irradiance of TSS, d) Direct irradiance of TSS, e) Global irradiance of UV-A, f) Direct irradiance of UV-A, g) Global irradiance of UV-B, h) Direct irradiance of UV-B.*

shown in Figure 3.1. The irradiance data, which are sampled in 10 seconds, are averaged over 10, 20, 30 and 60 minutes. The results of ε computations for 1995 (for the months May, June, July and August between 8 and 16 GMT) for the different averaging periods are shown in Figure 3.3. There are three types of ε events defined,

a) All possible ε events
b) Most likely ε events
c) ε events of not occluded Sun

Dotted bars in Figure 3.3 represent the percent of the total data for different averaging periods for *all possible ε events*. Standard error of the fit curves in Figure 3.1 for TSS, UV-A and UV-B and the instrumental uncertainties must be taken into consideration by determining the ε values. ε events having values above these uncertainties are called the *most likely ε events* (wiggled bars). The number of the *most likely ε events* is less than *all possible ε events*.

Solid bars (*ε events of not occluded Sun*) in Figure 3.3 show the ε events where the direct irradiance values are not significant lower than the fit of the direct irradiance. This fit is acquired from the direct irradiance measurements of the cloud-free days. As the instruments measuring the global irradiance, the instruments that measure the direct irradiances have an instrumental error of 3 % and 6 % for TSS and UV range, respectively. We have detected moments when the direct irradiance values lies above these uncertainty domains. Also the fit and instrumental error of the global irradiance is used to compute the ε values for those moments. The number of the ε values that fulfill these conditions lies as expected below the other two bars (solid bar). This condition for the direct irradiance is applied to ensure that the radiation is not absorbed and/or scattered by higher amounts of aerosols. The values of ε with this condition are then accompanied by high direct irradiance. Thus, *ε events of not occluded Sun* could arise from the contribution of reflections from the sides of clouds (called *CSIR events* by *Segal and Davis, 1991*) or from the contribution of diffuse irradiance. Difference between the wiggled bars and the solid bars in Figure 3.3 gives the percentage of the total data that is resulted from higher diffuse radiation in combination with lower direct radiation. ε values arising from the contribution of diffuse irradiance is lower than the ε values arising from the contribution of direct irradiance reflected from the sides of clouds. This is confirmed by the *ε events of not occluded Sun* that include the points of the maximum values of ε in the given averaging periods (solid lines in Figure 3.3).

As expected ε values are decreasing with increasing averaging periods. The maximum value of ε for the 10 seconds instantaneous measurements in TSS is about 73 %. Maximum value of ε determined by *Laird and Harshvardhan (1997)* for TSS is about 17 % using 2 minutes averaged data while *Segal and Davis (1991)* found a value of 30 %. In Figure 3.3 even the maximum value of ε of TSS using 10 minutes averaged data is higher than those values (40 %).

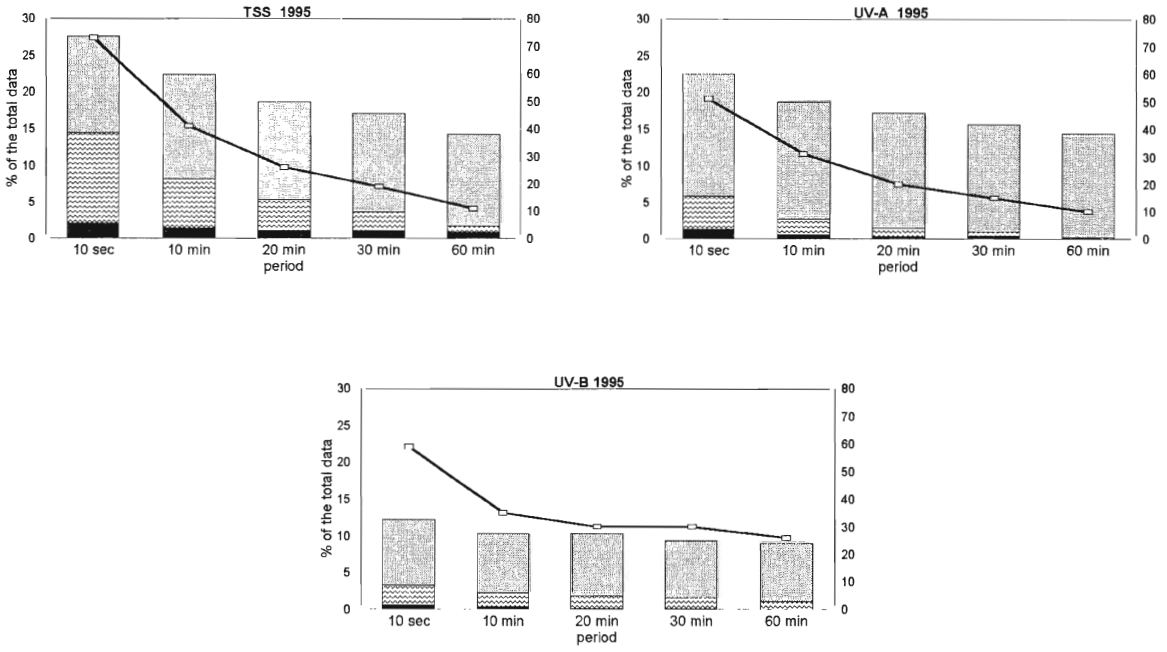

Figure 3.3. *Maximum ε values and the percent of data for different conditions for ε as a function of the averaging period for TSS, UV-A and UV-B, for the months May, June, July and August in 1995 between 8 and 16 GMT. See text for more details.*

Maximum value of ε is about 50 % and 60 % in the UV-A and UV-B range, respectively. *Laird and Harshvarhan (1997)* have observed a maximum of 8 % and 10 % in the UV-B and UV-A range, respectively. *Mims and Frederick (1994)* found a maximum ε of 29 % in UV-B. *Hayasaka et al. (1995)* has used aircraft measurements, and showed an ε on the order of a few percent.

Large variations in ε values are due to the differences in frequency of the irradiance data, used instruments and atmospheric conditions. The location of the measurements is another important factor influencing the ε values. The location of the study of *Mimms and Frederick* (Mauna Loa, Hawaii, at 3,4 km above see level) is particularly favorable to detect ε events, as clouds frequently rise from the valley past the observatory during the afternoon.

The duration of ε events is climatologically and biologically important. *Segal and Davis (1991)* suggested that ε events must have large duration in order to be climatological significant. For the three different uncertainty conditions are also the duration of ε events computed. In Table 4.1 these values are shown. *Segal and Davis (1991)* detected maximum durations between 0.25 and 0.50 hours. From our dataset and the choice of the cloud-free reference, maximum duration for various spectral ranges is 12 – 18 minutes for the *ε events of not occluded Sun.* Maximum duration of ε events is about half an hour for *most likely ε events*.

		maximum duration of ε events in hours		
		All possible ε events	*Most likely ε events*	*ε events of not occluded Sun*
Spectral Region	TSS	4.5	0.6	0.3
	UV-A	2.7	0.4	0.3
	UV-B	4.1	0.5	0.2

Table 3.2. *Maximum Duration of the ε events in 1995 for TSS, UV-A and UV-B.*

There is also a wavelength dependence of the ε events. Highest maximum ε value is in the TSS and lowest in the UV-A range for the 10 seconds instantaneous measurements (Figure 3.3). Maximum values of ε for TSS decreases stronger than UV-A and UV-B with increasing averaging periods. For averaging periods > 10 minutes maximum values of ε are of the same order for TSS and UV-A. In the UV-B region, the maximum values of ε decrease little with increasing averaging periods. For the averaging periods ≥ 10 minutes, the course of the maximum values of ε is about constant in the UV-B range and the number of *ε events of not occluded Sun* is very small for the averaging periods >10 minutes.

The percent of data for which ε > 0, decreases for shorter wavelengths. If the uncertainties of the fit and instrumental errors of the global irradiances are considered the percent of the data decreases still for shorter wavelengths for averaging periods up-to 20 minutes. In the UV-B, the percent of the data is almost constant for the different averaging periods. There can different reasons thought to explain this. One of it is that the *RAF* correction factors used in this study to eliminate the influence of the ozone column amount are overestimated. We have used the ozone column amount values of 12.00 GMT for the whole day and the *RAF* values are acquired from a model called TUV. Actually, we ought to use the appropriate ozone column amounts for each measurement for higher accuracy. The *RAF* values that result from the TUV model have also an uncertainty.

If we assume that the *RAF* values are correct, the reason for the almost constant percent data in the UV-B for different averaging periods is the wavelength dependence of the clouds and aerosols. Diffuse radiation in the cloud-free part of the sky arises from molecular (Rayleigh) scattering. Diffuse radiation from the cloud particles arises from Mie scattering. The aerosol amounts and properties are varying slower than the cloud properties. The ε events in the UV-B could be caused by the contribution of the enhanced diffuse radiation by Rayleigh and Mie scattering and because of its slow variation, these events could maintain longer. The decrease in the percent data that exhibit ε events in UV-B above the uncertainty of the fit and instrumental

errors is decreasing very slowly. If the restriction on the direct irradiance is applied then the percent of data decreases slowly too, but it holds up at 20 minutes averaging period. Obviously, some caution is required when interpreting wavelength dependence of the ε events.

4. A Simple Model for Cloud Coverage

4.1. Theory

Clouds and aerosols have effects on the measured irradiances that are relatively independent of wavelength. Surface reflections, although not observed directly by an upward-facing instrument, can increase the diffuse sky radiation through back scattering of upwelling radiation. Figure 4.1 (*Madronich et al, 1997*) shows the sensitivity of UV radiation to changes in various individual factors including clouds. In this Figure, we see that clouds have most effect on the transmission of the solar radiation. The net result may be more complex if more than one of these individual factors are superpositioned. For example, if the effect of surface albedo and the clouds are included, the radiation reducing property of the clouds in the presence of a highly reflecting surface may be relatively small even for thick cloud cover (*Stamnes et al, 1991*), because of the trapping of the radiation between the clouds and the Earth's surface.

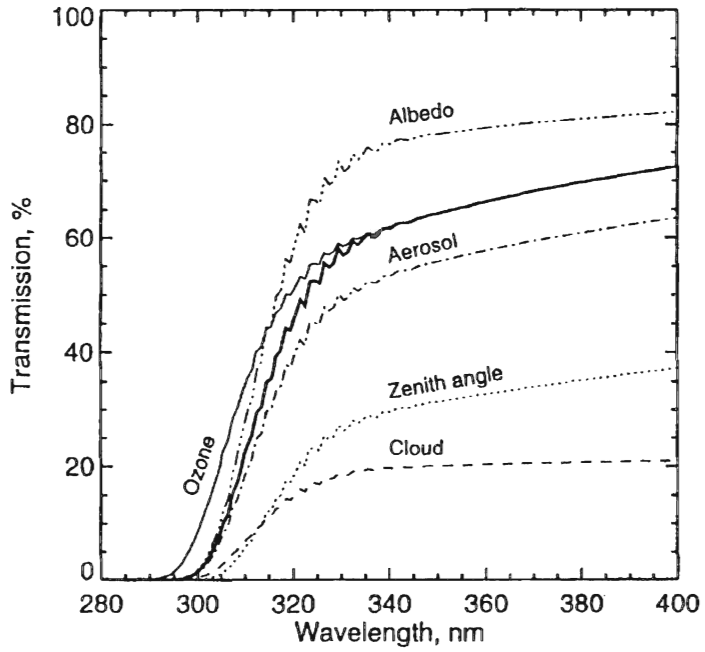

Figure 4.1. *Spectral transmission of different model atmospheres. The thick line gives results for down-welling surface irradiance calculated for 30° SZA, cloud-free and no aerosols, total ozone column of 300 DU and surface albedo of 5 %. Thin lines show the effects of changing these atmospheric conditions individually: Surface albedo increased to 60 %, total ozone column reduced to 150 DU, tropospheric aerosol visibility decreased to 10 km, SZA increased to 60°, and cloud layer with an optical depth of 32 included between 5 - 7 km.*

Partial cloudiness is extremely difficult to model, due to both the inherent three-dimensional nature of the problem, and to the infinitive variety of different morphologies of the cloud field. Clouds usually reduce radiation, but there is also the possibility of attaining higher values (ε events) of irradiance than at a cloud-free day. These enhancements are attributed to the reflections from the sides of the clouds (*Mims and Frederick, 1994*) and sum of the direct and increased diffuse irradiance. Figure 3.2a shows the global irradiance for cloud-free day (solid line) and for a partial cloudy day (dashed line) measured in De Bilt.

Here we introduce two simple models that the cloud coverage approximates with use of the irradiance data and the importance of the diffuse radiation illustrates. Global irradiance is the sum of the diffuse and the direct components of the irradiance,

$$E_{\mathrm{glb}}^{clr} = E_{dir}^{clr} + E_{dif}^{clr} \qquad \text{For cloud-free sky} \qquad (4.1.1)$$

$$E_{\mathrm{glb}}^{cld} = E_{dir}^{cld} + E_{dif}^{cld} \qquad \text{For overcast sky} \qquad (4.1.2)$$

Total irradiance can be estimated by superimposing the components E_{dir}^{clr}, E_{dif}^{clr}, E_{dir}^{cld} and E_{dif}^{cld} in proportion to the fraction of the sky, N, that is covered by clouds (*Nack and Green, 1974*). In Figure 4.3 are these components illustrated. E_{dir}^{cld} is smaller for thick clouds than E_{dir}^{clr}, due to the attenuation of the solar radiation. Because of the diffuse radiation that result from transmission of the solar radiation incident on the top of the clouds, E_{dif}^{cld} (arising from Mie scattering) may well be larger than E_{dif}^{clr} (arising from Rayleigh scattering). Clouds transmit a significant fraction of the sunlight that impinges on the cloud tops, and are therefore brighter, as seen from the ground, than the cloud-free part of the sky. At the same time, if the instruments that measure the global irradiance are exposed to the direct irradiance from the cloud-free part of the sky, the global irradiance measurements can result in substantially larger values than at a completely cloud-free sky. This is dependent on the cloud types. Cumulus clouds are one of the types of clouds that look brighter than the cloud-free part of the sky.

Complex effects such as scattering from the cloud sides and the influence of the clouds on the diffuse radiation in the cloud-free part of the sky is neglected. Only the radiation from the cloud base is contributing to the total irradiance. With these approximations,

$$E_{\mathrm{glb}}^{sun} = E_{dir}^{clr} + NE_{dif}^{cld} + (1-N)E_{dif}^{clr} = E_{\mathrm{glb}}^{clr} + N(E_{dif}^{cld} - E_{dif}^{clr}) \qquad (4.1.3)$$

$$E_{\mathrm{glb}}^{shd} = E_{dir}^{cld} + NE_{dif}^{cld} + (1-N)E_{dif}^{clr} = E_{\mathrm{glb}}^{cld} - (1-N)(E_{dif}^{cld} - E_{dif}^{clr}) \qquad (4.1.4)$$

E_{glb}^{sun} = Global irradiance when the Sun is not occluded.

E_{glb}^{shd} = Global irradiance when the Sun is occluded.

Global irradiance fluctuates between values exceeding completely cloud-free day values by $N(E_{dif}^{cld} - E_{dif}^{clr})$ and values of fully overcast sky irradiance by $(1-N)(E_{dif}^{cld} - E_{dif}^{clr})$.

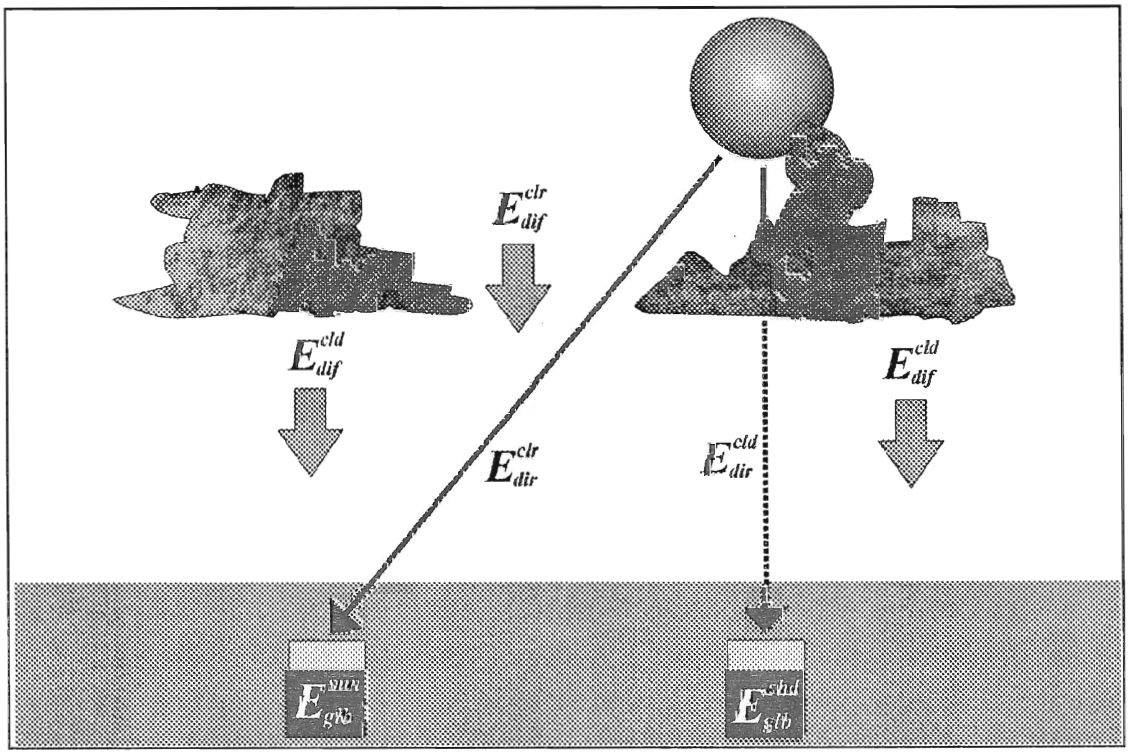

Figure 4.2. *Schematic illustration of the downward radiation for occluded and not occluded Sun for partial cloudy condition.*

If we assume that clouds are moving fast enough that within a given period the E_{glb}^{sun} and the E_{glb}^{shd} are at least detected once, we can approximate the weighted average of E_{glb}^{sun} and E_{glb}^{shd} as follows:

$$E_{glb}^{ave} = NE_{glb}^{shd} + (1-N)E_{glb}^{sun} \tag{4.1.5}$$

With use of above equations, it is possible to determine the cloud coverage N from our data.

$$N = \frac{E_{glb}^{sun} - E_{glb}^{ave}}{E_{glb}^{sun} - E_{glb}^{shd}} \tag{4.1.6}$$

4.2. Model 1

Model 1 computes the cloud coverage (N_{mod1}) for every 10 minutes interval with equation 4.1.6, using the direct and global irradiance data sampled in 10 seconds, applied to TSS. Direct irradiance measurements are used to determine whether the Sun is occluded or not occluded. If the Sun is not occluded, the instruments measuring the irradiance are exposed to the direct solar beam. Then the direct irradiance has relatively higher values than when the Sun is occluded. These moments are selected as moments of not occluded Sun. If the thicker clouds are replaced by thinner clouds then the direct irradiance has relatively higher values. Also these moments are considered as moments of not occluded Sun while the Sun is behind the clouds. In this model global irradiance values are used as E_{glb}^{sun} when the direct irradiance is maximum.

E_{glb}^{ave} is the average value of the global irradiance in the 10 minutes interval. This model is applied to the data of 1995 (for the months May, June, July and August between 9 and 16 GMT). The results of this model are compared with the hourly synoptic observations of the cloud coverage (N_{syn}) shown in Figure 4.3.

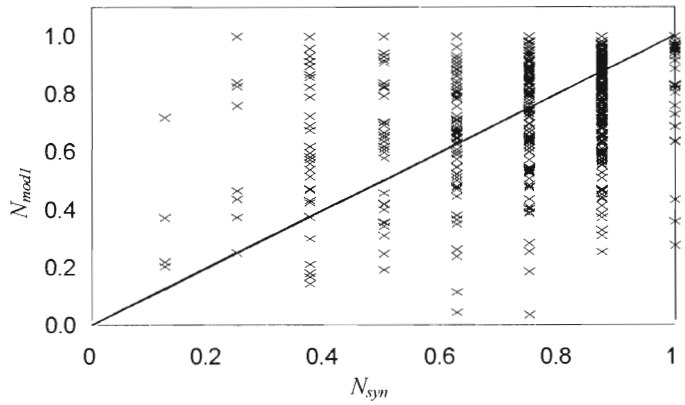

Figure 4.3. *Cloud coverage determined with model 1 as a function of reported (every hour) cloud coverage.* $N_{mod1} = (1.003 \pm 0.006)\, N_{syn}$ *, Standard error of* $N_{mod1} = 0.17$, $R^2 = 0.270$

Average values of global irradiance when the direct irradiance is below 5 W/m^2 is used as E_{glb}^{shd}. This limit is obtained from the mean value of the direct irradiance when the Sun is occluded. For this purpose fully overcast days are selected from our dataset and the mean value of the direct irradiance is calculated. If there are no values of direct irradiance below 5 W/m^2 in the 10 minutes interval there could no values detected for E_{glb}^{shd}. For these intervals, no N_{mod1} values are computed. Because of the use of direct irradiance values to select E_{glb}^{shd} and E_{glb}^{sun} values, it is possible that $E_{\mathrm{glb}}^{shd} > E_{\mathrm{glb}}^{ave}$. Points like this give a negative N_{mod1}. These values of N_{mod1}

are not used. Therefore, there are fewer points available to make a linear fit from the origin (Figure 4.3).

4.3. Model 2

Model 2 uses only the global irradiance data to compute the cloud coverage (N_{mod2}) for every 10 minutes. E_{glb}^{sun} is equal to the maximum value of the global irradiance and E_{glb}^{shd} is the average value of the points satisfying $E_{glb} < 0.9E_{glb}^{clr}$ in the 10 minutes interval. Moments when values of the global irradiance is lower than 90 % of the cloud-free reference, are considered as occluded Sun positions. This model is also applied to TSS as model 1 and the results of this model for 1995 are shown in Figure 4.4. E_{glb}^{ave} is the average value of the global irradiance in the 10 minutes interval. Due to the selection criterion E_{glb}^{shd} is always smaller than E_{glb}^{ave} and this gives positive N values, unlike model 1. Therefore for this model are more points available to make a linear fit from the origin (Figure 4.4).

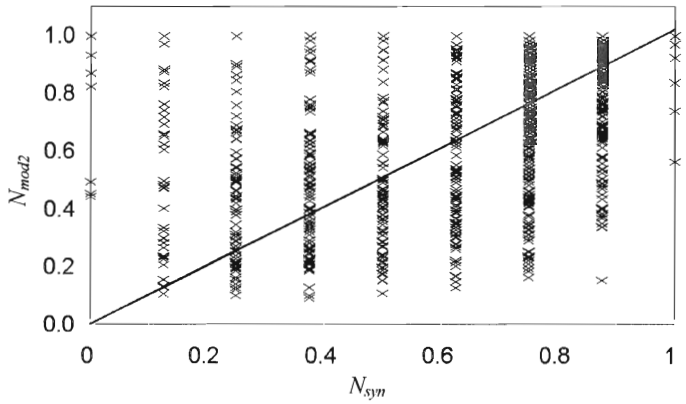

Figure 4.4. *Cloud coverage determined with model 2 as a function of reported (every hour) cloud coverage.* $N_{mod2} = (1.021 \pm 0.008)\, N_{syn}$, *Standard error of* $N_{mod2} = 0.23$, $R^2 = 0.295$

Model 1 fails when it is applied to the lower cloud coverage (Figure 4.3). There are less points plotted in the $0 < N_{syn} < 0.75$ domain than for model 2 (Figure 4.4). Model 1 uses a heavy criterion for direct irradiance (<5 W/m^2) to select E_{glb}^{shd} data. There were many data points that do not satisfy this criterion. If the cloud coverage is low, the direct irradiance may be higher than 5 W/m^2 during 10 minutes or longer periods. In this situations N_{mod1} has no value.

The linear fit from the origin of model 1 is more accurate than model 2 due to the standard error and R^2 of the fits. Model 1 computes the higher cloud coverage's better than model 2, but

model 2 computes all the cloud coverage with a certain accuracy because of the selection criterion for E_{glb}^{shd} .

4.4. An empirical method for cloud coverage

From the available synoptic reports, *Holtslag and van Ulden (1980)* tried to estimate the hourly averages of the global irradiance. They have showed that global irradiance can be estimated relatively accurate only from SZA and total cloud coverage. Furthermore, their method is tested with the data of 1989 in De Bilt and more accuracy is added by using shadowing cloud coverage instead of total cloud coverage (*Nolet, 1991*). We are interested in the reverse procedure, i.e. in the estimation of the cloud coverage from the irradiance data. The formula that is used to estimate the global irradiance is reformulated for the cloud coverage (N_{emp}),

$$N_{emp} = \sqrt{c\left(1 - \frac{E_{\mathrm{glb}}}{S\mu_0(a + b\mu_0)}\right)} \qquad (4.4.1)$$

where S =1353 W/m^2 (solar constant),
a = 0.62, b = 0.22 and c = 0.70 are the empirical determined constants.

E_{glb} is here the hourly averaged global irradiance of TSS. We calculated the N_{emp} with our data and plotted these against the synoptic data in Figure 4.5. The slope of the linear fit from the origin is very low. This method underestimates the cloud coverages and the R^2 shows that this method compares better with synoptic cloud cover reports than model 1 and model 2.

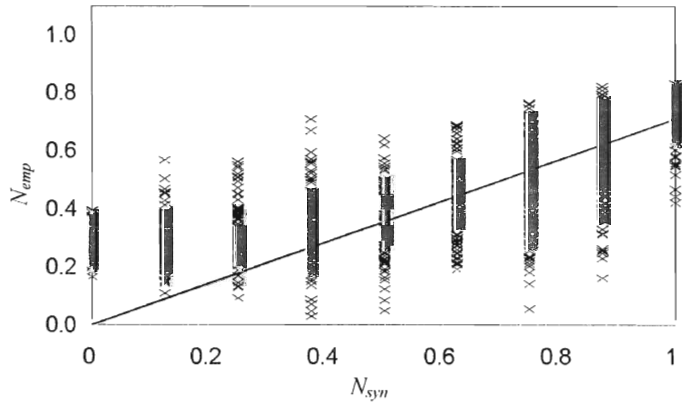

Figure 4.5. *Cloud coverage estimated with the empirical formula developed by Holtslag and van Ulden as a function of reported (every hour) cloud coverage.*
N_{emp} = (0.712±0.005) N_{syn} , Standard error of N_{emp}= 0.14, R^2 =0.485

4.5. Cloud transmission

Cloud transmission is defined as the reduction of irradiance under completely overcast conditions relative to the completely cloud-free conditions namely, $E_{\text{glb}}^{cld} / E_{\text{glb}}^{clr}$. With use of equation 4.1.4 we get for cloud transmission,

$$T_c = \frac{1}{E_{\text{glb}}^{clr}}\left[E_{\text{glb}}^{shd} + (1-N)(E_{dif}^{cld} - E_{dif}^{clr})\right] \qquad (4.5.1)$$

Cloud transmission T_c is only possible to compute if the Sun is behind the clouds, i.e. if E_{glb}^{shd} has a value achieved from model 1 or 2. If cloud coverage N is equal to 1 then T_c is easily to compute from our dataset, with use of the E_{glb}^{shd} (achieved from model 1 or 2) and E_{glb}^{clr} (achieved from cloud-free reference) values. For the other cloud covers, it's difficult to apply equation 4.5.1, because E_{dif}^{cld} and E_{dif}^{clr} values are not direct to obtain from the dataset. We can make some approximations to refer values for these variables in TSS. In Figures 3.2c and 2.5b, we see that the diffuse irradiance on a cloud-free day is about constant between 9 and 16 GMT in TSS, and has a value of about 80 W/m^2. In addition, the diffuse irradiance on the other days is about constant. Thus, we can refer the mean value of the diffuse irradiance on these days as E_{dif}^{clr}. Nevertheless, the determination of the value of E_{dif}^{cld} forms a problem. If we apply this equation to TSS, we can use the approximation $E_{\text{glb}}^{cld} \cong E_{\text{glb}}^{shd} / N$. This is derived from 4.5.1 assuming that E_{dir}^{cld} and E_{dif}^{clr} are relatively small compare to E_{glb}^{shd}. In the next chapter T_c values are computed for some selected days.

Wavelength dependence of T_c is rather weak for completely overcast sky. The average transmission under partly cloudy skies, $E_{\text{glb}}^{ave} / E_{\text{glb}}^{clr}$, is also only weakly dependent on wavelength. Because of increasing Rayleigh scattering, at shorter wavelengths increases diffuse irradiance relative to the global irradiance. Diffuse irradiance acquired by subtracting direct irradiance from global irradiance in Figure 3.2 is about 50 % and 65 % of global irradiance in UV-A and UV-B, respectively, while this is about 10 % in TSS. Thus if it is not completely overcast the diffuse components in equation 4.5.1 becomes more significant at shorter wavelengths and approximations that are explained above to compute the T_c from the TSS data are not applicable on the UV data.

5. Case Studies

We have selected seven partial cloudy days from our dataset to study the ε events and the influence of partial cloudiness on the irradiance values and its spectral distribution. In Table 5.1 are also the general characteristics of the three cloud-free days (of which only the days of 1995 are used to construct the cloud-free reference of the UV range). Selection of these days was made by looking to the duration of ε events and the ε values in all spectral ranges.

Case Study Days													
Day number	Date	Wind		Relative Humidity (%)	Sunshine (hours)	Visibility (km)	Clouds			Last precipitation (...days ago)	ε Moments (GMT)		
		Direction	Speed (m/s)				Type	Height (km)	Coverage (N)		TSS	UV-A	UV-B
1	22 July 1995	NW	3	62	10	30	Cu	800	0.375	1	11-15	12-15	8-9, 13-14
2	5 August 1995	NE	3	62	14	30	Cu	200	0.250	8	8-11	-	9
3	26 August 1995	NW	4	64	5	32	Cu	900	0.625	0	9, 11-12	9, 11-13	9-13
4	30 August 1995	NW	5	63	9	32	Cu	100	0.500	0	9-15	8-15	-
5	28 May 1996	NW	3	56	11	35	Cu	900	0.500	1	9-13, 15	8-16	8-15
6	15 June 1996	NE	3	48	15	35	Cu	700	0.375	4	8-12	8-13	8-12
7	16 July 1996	N	5	62	8	32	Cu	850	0.750	6	8, 10	8-16	8-15
Cloud – Free Days													
8	25 July 1995	NE	4	49	15	34	-	-	-	4	-	-	-
9	1 August 1995	NE	4	38	13	34	-	-	-	5	-	-	-
10	20 July 1996	vari-able	2	37	15	34	-	-	-	9	-	-	-

Table 5.1. *General characteristics of ancillary data for case study days that exhibit long duration of ε events and high ε values, and cloud – free days. Wind speed, wind direction, relative humidity and visibility are averaged between 8 and 16 GMT. Cloud type is the lowest and most covered cloud type of the days.*

5.1. "16 July 1996"

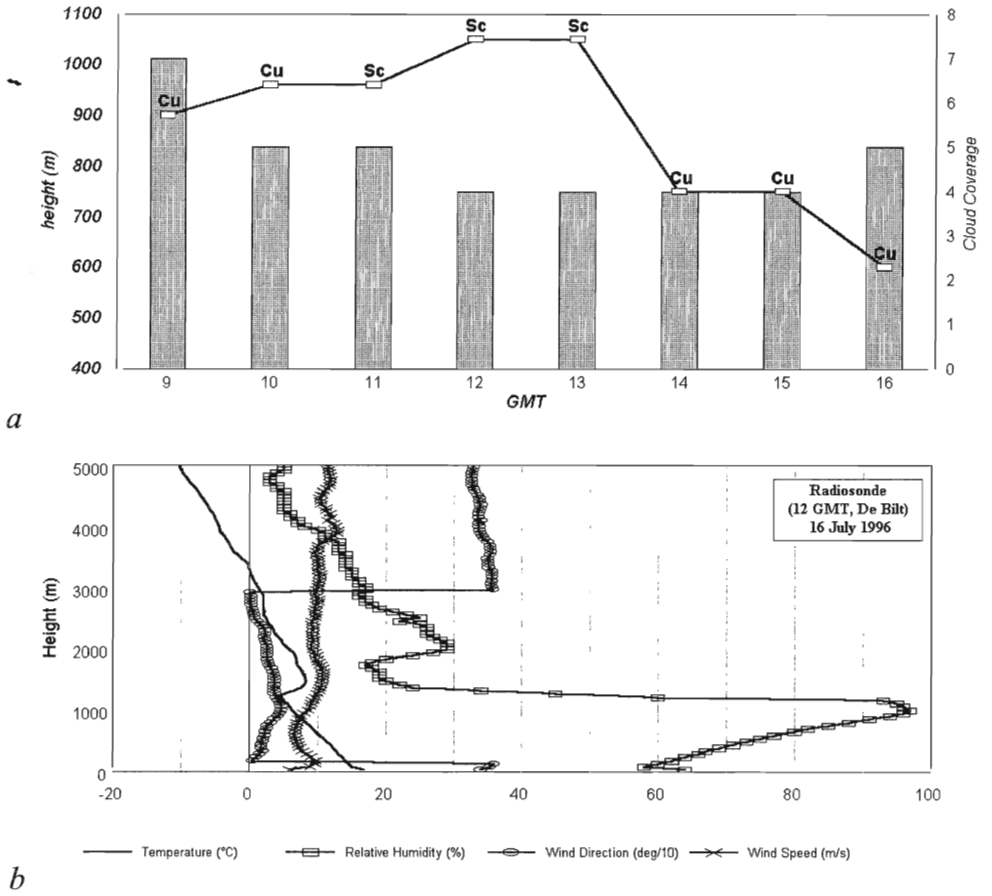

a

b

Figure 5.1. a) *Synoptic data of 16 July 1996. Cloud base heights (solid lines), cloud types (on this day; Cu, Sc) and total cloud coverage (dotted bars).*
b) *Radiosonde data of 16 July 1996.*

16 July 1996 (day 7) is one of the interesting days in our dataset exhibiting significant ε events in TSS. However, the absolute data of 1996 in the UV region can not be used for the calculation of enhancements, as explained in Chapter 2. The cloud-free reference equation is based on data of 1995 and can not be applied to the UV data of 1996. ε values and duration of ε of 16 July 1996 can only be computed with another cloud-free reference. Instead of using the cloud-free reference equation (3.1.1), nearest cloud-free day measurements, which is 20 July 1996 (day 10) can be used to compute ε values and durations of ε events. For this purpose, ratio (r) of 10 seconds instantaneous and 10 minutes averaged irradiance measurements of day 7 with respect to the cloud-free day (day10) between 9 and 16 GMT are plotted in Figure 5.2.

Synoptic data of day 7 shows that only cumulus like clouds are observed (Figure 5.1a). Radiosonde measurements of De Bilt at 12 GMT shows that the wind direction between 100 and

3000 meters is North. There is an inversion at about 1000 meters in relative humidity and temperature.

Fluctuations in 10 minutes averaged irradiances are less strong than 10 seconds instantaneous irradiances due to the weakening in fluctuations of the irradiances with increasing averaging period (Figure 5.2). Difference between ε and r is that ε is the enhancement of global irradiance relative to the cloud-free reference in percent and r is the ratio of the measurements relative to the reference day. If we assume that day 10 is a good approximation of the cloud free-reference, than ε values of day 7 can be obtained by (1-r)×100, using only the global irradiances. In global component of TSS the maximum value of r is about 1.6 and 1.3 (ε = 60 % and 30 %) around 16 GMT for 10 seconds data and 10 minutes data, respectively (Figure 5.2a). In average, r-values of the direct irradiances are increasing in all spectral ranges in the course of the day. But the anomalous increase of r values of the direct irradiances especially in the UV region is remarkable (Figure 5.2b, e, h), direct irradiances are more then 2 times higher on the partial cloudy day than on the cloud-free day in the UV range. Diffuse irradiance is in average decreasing in time (with the highest decrease in TSS and a very weak decrease in UV-B), while the direct irradiance is increasing (Figure 5.2c, f, i). The ratio of day 7 relative to day 10 is not favorable for examining whether enhancements are mostly imputed to the contribution of diffuse or direct irradiance. The decrease in relative diffuse irradiance is compensated by increase in relative direct irradiance especially on the cloud-free day. For this reason, we have zoomed into the periods where one of the components of the global irradiances are constant on the cloud-free day. In Figure 5.3 such a period is shown between 9 and 10 GMT. There are no r values of global and direct irradiance greater than 1, using 10 minutes data, in all spectral ranges (Figure 5.3a, d, g). Variation in diffuse irradiance of TSS is low by comparison with diffuse irradiance in Figure 5.2. 10 seconds data exhibits r values of global irradiances in TSS greater than 1. Direct irradiances of 10 seconds in TSS on day 7 is not exceeding direct irradiances on day 10 and r of diffuse irradiance in TSS is quite high. The enhancements in global irradiance (r values >1) are in this situation attributed to the fluctuations in the direct irradiance, because diffuse irradiance is about constant, only the direct irradiance is fluctuating and the enhancements in global irradiance are occurring exactly at the same moments when the direct irradiances are increasing. Also, the 10 minutes data of direct irradiance has approximately the same course as global irradiance.

However, in the UV-A, diffuse irradiance of 10 seconds periods is fluctuating more than in TSS (Figure 5.3f). This may be due to the Rayleigh scattering below the clouds, which is increasing at shorter wavelengths. This causes fluctuations in the diffuse UV-A irradiance that follows the fluctuations in the direct UV-A irradiance. Increases in global UV-A irradiances also coincide with the increases in the direct UV-A irradiances (Figure 5.3d, e). Like in TSS, plotted 10 minutes data is also confirming the increase of global irradiance with corresponding increase in direct irradiance.

Like in the UV-A the diffuse irradiance in UV-B of 10 seconds periods is fluctuating more than in TSS, but less than in UV-A (Figure 5.3i). This could be due to the ozone absorption of the scattered radiation. The enhancements in UV-B are low and in general, they are coinciding

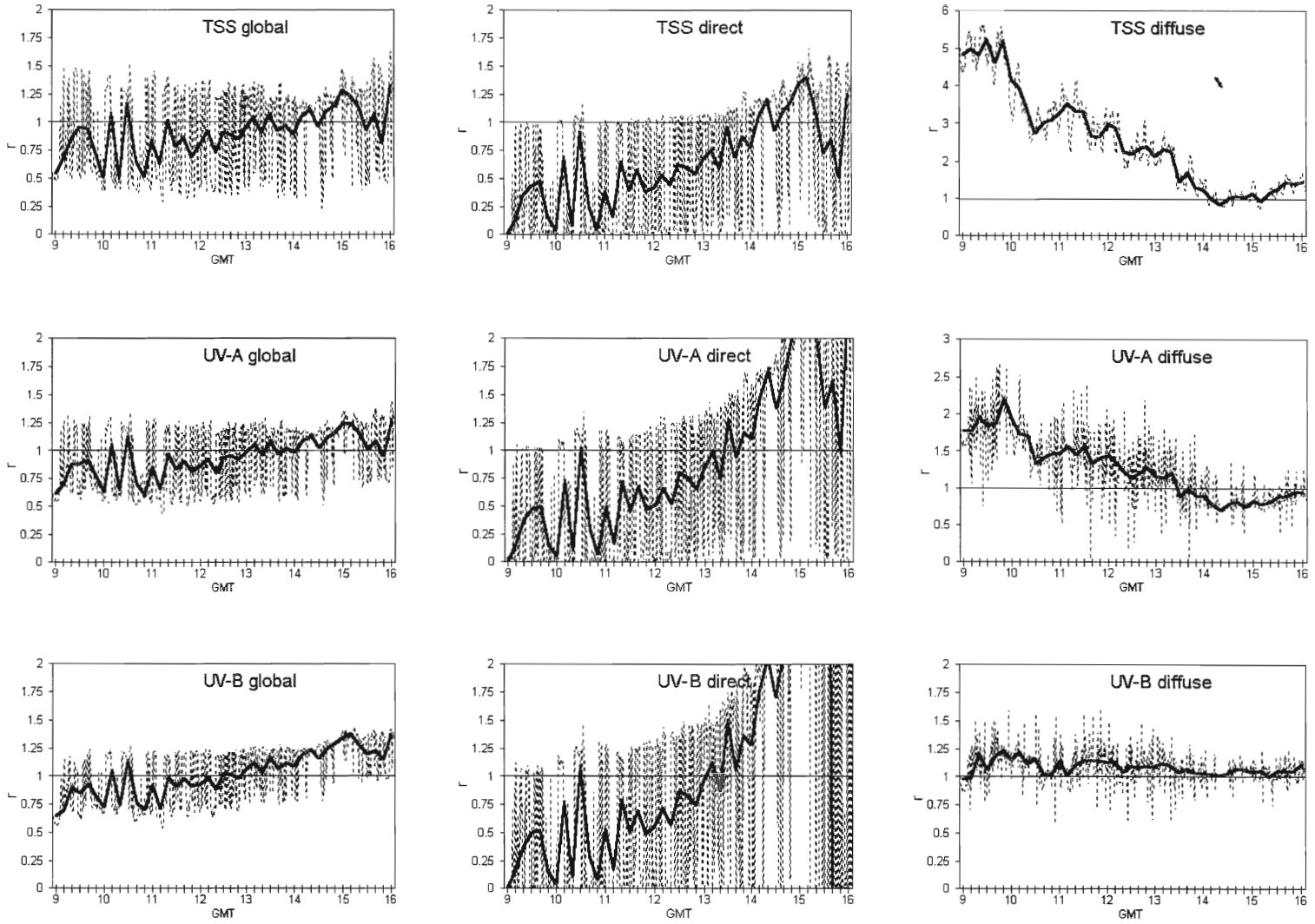

Figure 5.2. *Ratio (r) of global, direct and diffuse irradiances in TSS, UV-A and UV-B (corrected to 300 DU with RAF method) between 9 and 16 GMT for 10 seconds instantaneous measurements (dashed lines) and 10 minutes averaged values (solid lines). 16 July 1996 (308 DU) in proportion to 20 July 1996 (323 DU).*

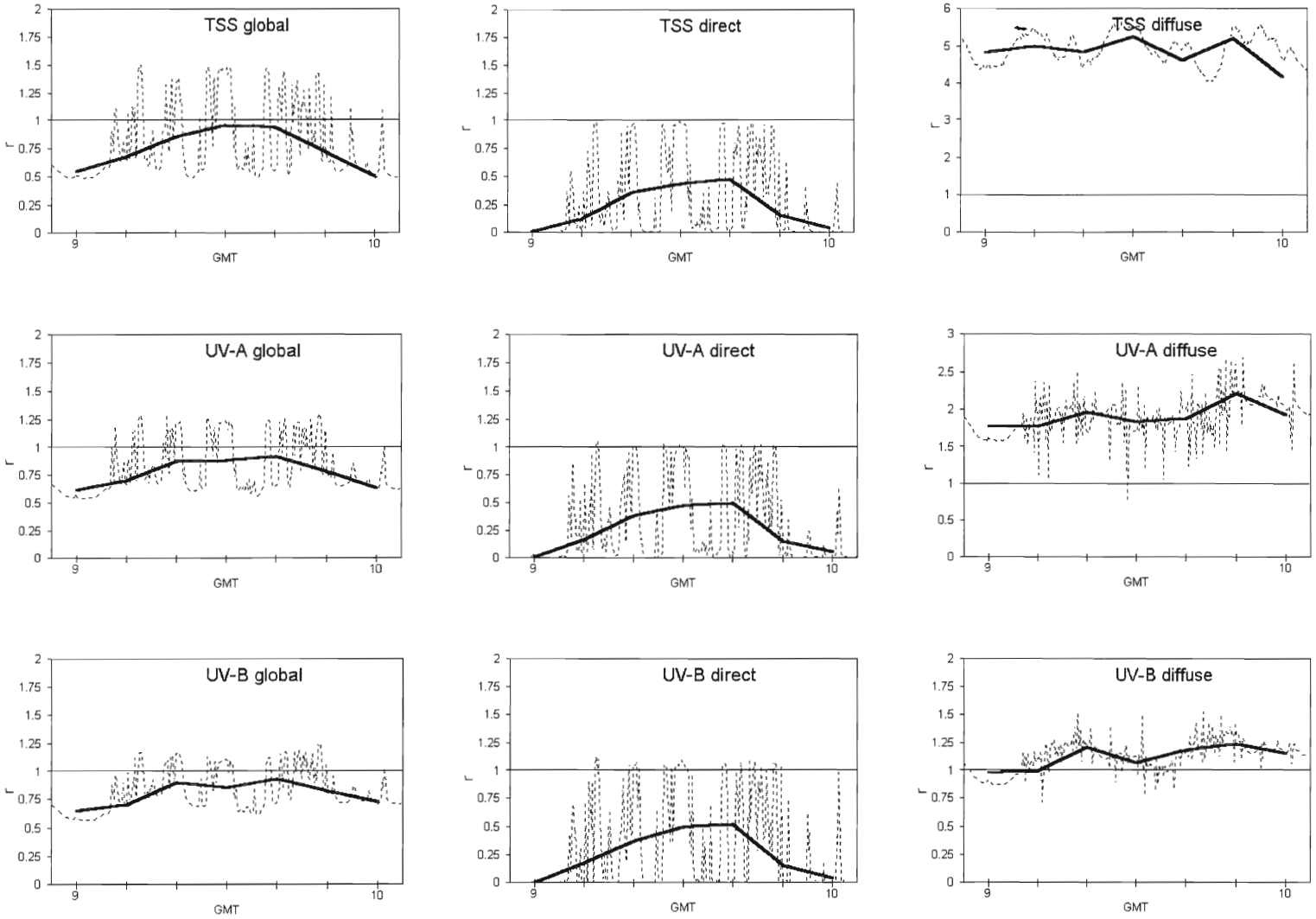

Figure 5.3. *Ratio (r) of global, direct and diffuse irradiances in TSS, UV-A and UV-B (corrected to 300 DU with RAF method) between 9 and 10 GMT for 10 seconds instantaneous measurements (dashed lines) and 10 minutes averaged values (solid lines). 16 July 1996 (308 DU) in proportion to 20 July 1996 (323 DU).*

with the increases in the direct irradiances, but not so consistent as in TSS and UV-A. The course of 10 minutes data of direct irradiance is not confirming the increase in global irradiance, rather the course of the diffuse irradiance resembles the increase in global irradiance. The contribution of the diffuse component on the enhancements of global irradiance is more important than the direct component with decreasing wavelength.

r values of diffuse irradiances are decreasing (Figure 5.3c, f, i) and r values of direct irradiances increase slightly with decreasing wavelength (Figure 5.3b, e, h). This is attributed to the wavelength dependence of the distribution of diffuse and direct irradiance. Diffuse irradiance is increasing relative to the global irradiance with increasing wavelength. Diffuse irradiance is high on a cloud-free day (denominator of r values of diffuse irradiance) but diffuse irradiance on a partial cloudy day is not much higher (numerator of r values of diffuse irradiance) at shorter wavelength ranges such as UV-A and UV-B. Another reason of this decrease is the aerosol contents of these days. On the cloud-free day, the synoptic conditions (Table 5.1) show that on this day more aerosol amount may be present than on the partial cloudy day. On day 10 the wind direction was variable with a low wind speed and there was no precipitation observed since 9 days. Northern wind with a higher speed and precipitation of 6 days ago is recorded on day 7. Northern winds advect clean air to De Bilt. Easterly winds bring more polluted air because of the Eastern industrial regions. Decrease of r values of diffuse irradiance with decreasing wavelength may be strengthened by these synoptic situations.

5.2. Other Days

Case study days in Table 5.1 show that ε events are possible in the presence of cumulus clouds (Cu). This is also confirmed by *McCormick and Suehrcke (1990)* and *Mims and Frederick (1994)*. The height (h) of the clouds and the coverage (N) is also determinative for the ε events. On these days there are no ε events detected for clouds higher than 1500 m and cloud coverages ≤ 0.125. A suitable geometry of clouds is required for the ε events. With some caution, we have interpreted the combination of N and h from our ε computations for the whole dataset. Mostly, the ε events are observed within the combinations $0.125<N\leq0.625$ with $100\ m\leq h\leq900\ m$ and $0.625<N\leq1$ with $900\ m<h\leq1500\ m$.

Wind direction on the days of ε events is mostly North. Also the case study days in Table 5.1 verifies this. Northern wind brings relatively cleaner air above The Netherlands. Absorption and back scattering of solar radiation is then relatively low, causing for the higher probability of ε events.

In Figure 5.4 the ε values of the case study days are plotted as a function of SZA for TSS, UV-A and UV-B obtained from 10 minutes averaged data. All ε values are plotted, i.e. the uncertainties in the instruments and the condition for direct irradiance are not taken into account. The density of ε values decreases with increasing SZA, and the maximum value of ε lies around

45^0 in all spectral ranges. The possibility of a suitable geometry for ε events is realized most for small SZA, because of the higher possibility of exposure of the instruments to the direct solar radiation. Detected ε values are decreasing with decreasing wavelength.

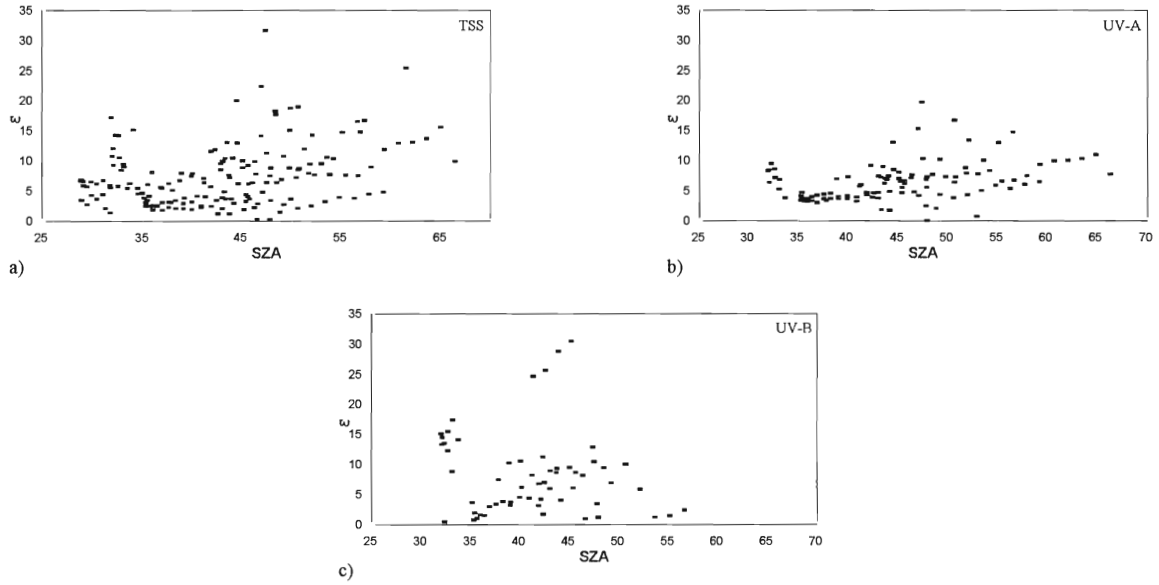

Figure 5.4. *ε Values of the 7 case study days for TSS (a), UV-A (b) and UV-B (c), attained from 10 minutes averaged data as a function of SZA. There is no error correction and condition for the direct irradiance applied and the ε values of 1996 in UV-A and UV-B are excluded.*

The relation of ε values with cloud coverage (N) can not be studied with hourly synoptic reports only, because of its low time resolution. Therefore, the N values acquired from model 1 or 2 are used. In Chapter 4.3 it is explained that model 1 computes the higher cloud coverages better than model 2, but model 2 computes all the cloud coverages with a certain accuracy. In Figure 5.5 is a plot of model 1 and 2 against synoptic reports shown. Just as for the other days, on the case study days model 2 has more points than model 1 (compare Figure 4.4 with Figure 4.5). Therefore, from now on only model 2 will be used.

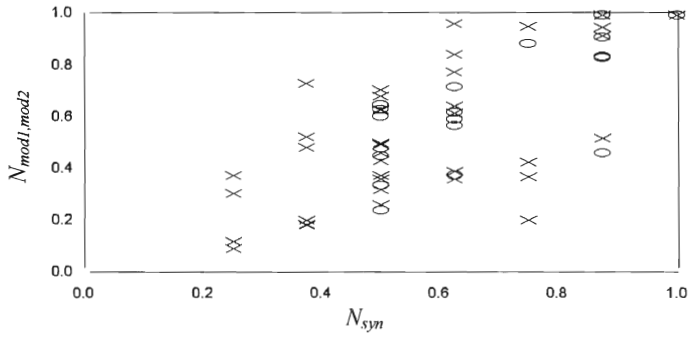

Figure 5.5. *Cloud coverage determined with model 1(O) and model 2 (X) as a function of hourly reported cloud coverage for the case study days in Table 5.1.*

In Figure 5.6 are the plots of ε values for TSS, UV-A and UV-B shown as a function of cloud coverage. Generally, ε values are decreasing with increasing cloud coverage. Negative values of ε refer to decrease of global irradiance on partial cloudy days relative to the cloud–free reference in percent. At about cloud coverage of 0.4, ε switches its sign. Thus, ε events are roughly only observed for cloud coverages lower than 0.4. There are more points in the TSS range than in the UV range. This is caused by the exclusion of the UV data of 1996.

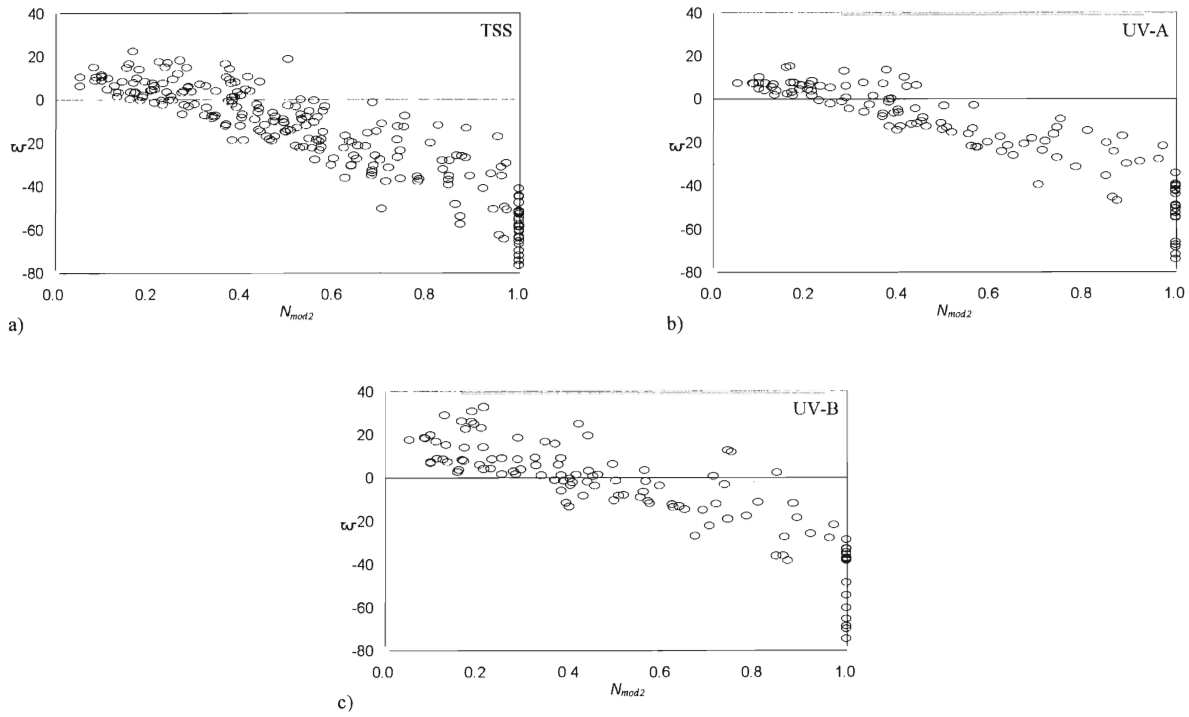

Figure 5.6. *ε values (10 minutes interval) of TSS (a), UV-A (b), UV-B (c) as a function of cloud coverage (N) for the selected 7 case study days.*

There are also cloud transmissions (T_c) computed for the selected 7 case study days, using the cloud coverages determined with model 2. As explained in Chapter 4.5, there are only irradiance values of TSS used. T_c values as a function of ε values for different spectral ranges are plotted in Figure 5.7. Completely overcast sky periods give a linear relation in all spectral ranges (points in the lower boundary of ε values in Figure 5.7). This is expected from the definition of T_c, which is the reduction of irradiance under completely overcast sky conditions relative to the completely cloud-free conditions namely, $E_{\mathrm{glb}}^{cld} / E_{\mathrm{glb}}^{clr}$. There are no ε values present for $T_c > 0.7$ in all spectral ranges, i.e. most of the ε events occur for thick clouds. Maximum values of ε are located about $T_c = 0.30$.

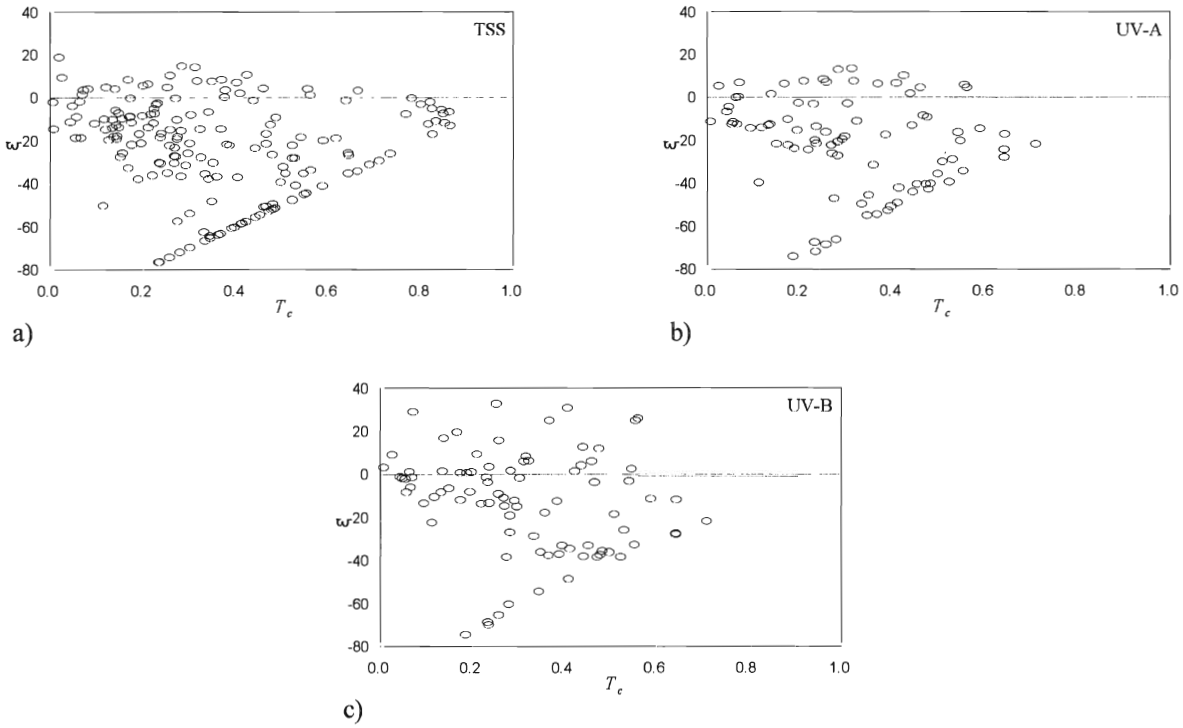

Figure 5.7. *ε values (10 minutes interval) of TSS (a), UV-A (b), UV-B (c) as a function of cloud transmission (T_c) for the selected 7 case study days.*

6. Conclusions

In this report, the enhancement of global irradiance with respect to the cloud-free values is studied, using the radiation data obtained from narrow band UV meters, pyranometers and pryheliometers located at KNMI, De Bilt. The measurements of TSS in 1995 and 1996 are used. The quality analysis has shown that the UV measurements of 1996 are shifted with an absolute value of up to 2 W/m^2 (UV-A), which is relatively high in the UV range.

Cloud-free references of global irradiance of TSS, UV-A and UV-B are constructed using global irradiance measurements of three days that fulfill the cloud-free criteria, which implies that the curves of global, direct and diffuse irradiance components of the whole spectral ranges have a smooth form. Absorption of UV-B irradiance by ozone formed a problem by constructing the cloud-free reference of the global UV-B irradiance. The accuracy of the cloud-free reference of global UV-B irradiance is improved with the *RAF* correction method, which estimates the UV-B irradiances for a reference total ozone column amount.

Enhancement over cloud-free values of global irradiances (ε) are detected with different methods. One of them is to compare the measurements of a cloud-free day with the measurements of the same day in another year when it was partial cloudy. There are ε values of 22 % and 16 % observed on 25 July 1996 with respect to 25 July 1995 in TSS and UV-A ranges, respectively.

ε values are computed for all measurements using the cloud-free reference equations. There are three types of ε events defined concerning the instrumental and cloud-free reference equation error, and direct irradiance measurements: *1) All ε events, 2) Most likely ε events, 3) ε events of not occluded Sun*. The number of ε events and maximum value of ε are decreasing with averaging periods in all spectral ranges with the slowest decrease in the UV-B range. Maximum value of ε is 73 %, 50 % 60 % in TSS, UV-A, UV-B, respectively. Maximum duration of ε events is about 30 minutes for *most likely ε events,* which includes the uncertainties in instrumental and cloud-free reference equation errors. *ε events of not occluded Sun* (i.e., the direct irradiance values are not significant lower than the fit of the direct irradiance) gives lower values for de number of *ε events* and duration of ε events.

Model 1 (using direct irradiance measurements) computes the higher cloud coverages better than model 2 (using global irradiance measurements), but it fails at lower cloud coverages, while model 2 computes all the cloud coverages with a certain accuracy because of more flexibility in the selection criterion for E_{glb}^{shd}. The empirical method of *Holtslag and van Ulden (1980)* underestimates the cloud coverages.

The absolute UV measurements of 1996 are not used. However, the ε events of 16 July 1996 can be studied with ratios of the measured irradiances with respect to the nearest cloud-free day, which is 20 July 1996. Several ε events occurred on 16 July 1996. In TSS and UV-A the

enhancements occur when the direct irradiance is increasing. The 10 minutes data of direct irradiance has the same course as the global irradiance. The enhancements in UV-B are low and in general, they are coinciding with increases in the direct irradiance, but not as consistent as in TSS and UV-A. In the UV-B, the course of diffuse irradiance resembles the increases in global irradiance more.

Our study showed that most ε events are observed when cumulus-like clouds are present. Mostly, the ε events are observed within cloud coverage (N) and cloud base height (h) combinations: $0.125<N\leq0.625$ with $100\ m\leq h\leq900\ m$ and $0.625<N\leq1$ with $900\ m<h\leq1500\ m$. All ε events are accompanied by northern winds, which bring relatively cleaner air above the Netherlands, causing for the higher probability of ε event because of less absorption and backscattering of the solar radiation.

The possibility of a suitable geometry for ε events is realized mostly for small SZA. The density of ε events is decreasing with increasing SZA, and the maximum value of ε is found around 45^0 in all spectral ranges.

The dependency of ε values on cloud coverage is studied with the results of model 2, which is sampled in 10 minutes. ε events are observed only for cloud coverages lower than 0.4 in the case study.

Maximum value of ε is observed for a cloud transmission of 0.30 and there are no ε values present for cloud transmission higher than 0.7 in all spectral ranges, i.e. most of the ε events occur for thick clouds.

7. Acknowledgements

I would like to thank the following people:

Michiel van Weele, Han van Dop, Ankie Piters, Hans Cuijpers and Casper Hofman.

8. References

Bodeker, G.E., and R.L. McKenzie, An algorithm for inferring surface UV irradiance including cloud effects, *J. Appl. Meteorol., 35*, 1860-1877, 1996.

Bordewijk, J.A., H. Slaper, H.A.J.M. Reinen, and E. Schlamann, Total solar radiation and the influence of clouds and aerosols on the biologically effective UV, *Geophys. Res. Lett., 22*, 16, 2151-2154, 1995.

Deluisi, J., Atmospheric ultraviolet radiation scattering and absorption, In: Solar ultraviolet radiation, Modelling measurements and effects (eds. C. S. Zerefos and A. F. Bais), *NATO ASI Series, series 1*: Global environmental change, vol.52, Springer, 65-85, 1997.

Frederick, J.E., and H. E. Snell, Tropospheric influence on solar ultraviolet radiation: The role of Clouds, *J. Climate, 3*, 373-381, 1990.

Hayasaka, T., N. Kikuchi, and M. Tanaka, Absorption of solar radiation by stratocumulus clouds: Aircraft measurements and theoretical calculations. *J. Appl. Meteorol., 34*, 1047-1055, 1995.

Holtslag, A.A.M., and A. P. van Ulden, Estimates of incoming shortwave radiation and net radiation from standard meteorologocal data, *KNMI, Sci. Rep., WR 80-6*, 16 pp., Royal Neth. Meteorol. Inst., De Bilt, 1980.

Jianzhong, M., and R. Guicherit, Effects of stratospheric ozone depletion and tropospheric pollution on UVB radiation in the troposphere. *Photochem. Photobiol, 66*, 3, 346-355, 1997.

Krotkov, N.A., P.K. Bhartia, J. R. Herman, V. Fioletov, and J. Kerr, Satellite estimation of spectral surface UV irradiance in the presence of tropospheric aerosols; 1. Cloud-free case, *J. Geophys. Res., 103*, 8, 8779-8793, 1998.

Kuik, F., Operationele UV-metingen bij het KNMI, *KNMI, Tech. Rep. TR-200,* 30 pp., Royal Neth. Meteorol. Inst., De Bilt, 1997.

Kuik, F., and H. Kelder, Spectral ultraviolet radiation measurements and correlation with atmospheric parameters, *KNMI, Sci. Rep., WR 94-05*, 40 pp., Royal Neth. Meteorol. Inst., De Bilt, 1994.

Laird, J.L., and Harshvardhan, Analysis of cumulus solar irradiance reflectance (CSIR) events. *Atmos. Res. 44,* 317-332, 1997.

Liu, S.L., S. A. McKeen, and S. Madronich, Effects of anthropogenic aerosols on biologically active ultraviolet radiation, *Geophys Res. Lett., 18*, 2265-2268, 1991.

Madronich, S., R. L. MvKenzie, M. M. Caldwell, and L. O. Björn, Changes in ultraviolet radiation reaching the earth's surface, *AMBIO*, 24, 3, 143-152, Royal Swedish Acedemy of Sciences, Stockholm, 1995.

Madronich, S., The atmosphere and UV-B radiation at ground level, In Environmental UV Photobiology (eds. Antony R. Young et all.), Plenum Press, New York, 1993.

Madronich, S., and S. Flocke, Theoretical estimation of biologically effective UV radiation at the earth's surface. In: Solar ultraviolet radiation, Modelling measurements and effects (eds. C. S. Zerefos and A. F. Bais), *NATO ASI Series, series 1*: Global environmental change ,vol.52, Springer, 23-48, 1997.

McCormick, P.G., and H. Suehrcke, Cloud-reflected radiation, *Nature, 345*, 773, 1990.

Mims, F.M., and J. E. Frederick, Cumulus clouds and UV-B, *Nature, 371,* 291, 1994.

Nack, M.L., and A.E.S. Green, Influence of clouds, haze, and smog on the middle ultraviolet reaching the ground, *Appl. Opt., 12*, 2405-2415, 1974.

Nolet, M.C., Dagsom van de globale straling, *KNMI, Tech. Rep., TR –138*0, 13 pp., Royal Neth. Meteorol. Inst., De Bilt, 1991.

Segal, M., and J. Davis, The impact of deep cumulus reflection on the ground level global irradiance. *J. Appl. Meteorol., 31*, 217-22, 1991.

Spencer, J.W., Fourier series representation of the position of the sun, *Search, 2,* 172, 1971.

Stamnes, K., J. Slusser, and M. Bowen, Derivation of total ozone abbundance and cloud effects from spectral irradiance measurements, *Appl. Opt., 30,* 4418-4426, 1991.

Appendix A

R^2

The degree of relationship between independent (x) and dependent (y) variables. With one independent variable, R^2 is the square of the correlation (r) between the two variables.

$$r = \frac{n\sum x_i y_i - \sum x_i \sum y_i}{\left[n\sum x_i^2 - \left(\sum x_i\right)^2\right]^{1/2}\left[n\sum y_i^2 - \left(\sum y_i\right)^2\right]^{1/2}} \quad \text{(A1)}$$

where n is the number of x or y values.

Estimated standard error of the dependent variable (y): S_y

The degree of deviation of observed y values from predicted values.

$$S_y = \sqrt{\left[\frac{1}{n(n-2)}\right]\left[n\sum y_i^2 - \left(\sum y_i\right)^2 - \frac{\left[n\sum x_i y_i - \left(\sum x_i\right)\left(\sum y_i\right)\right]^2}{n\sum x_i^2 - \left(\sum x_i\right)^2}\right]} \quad \text{(A2)}$$

Appendix B

Variation in the Earth-Sun distance

Because of the elliptical orbit of the Earth with the Sun at one of the foci, varies the Earth-Sun distance within the yearly cycle. This variation can be computed by,

$$\left(\frac{R_0}{R_n}\right)^2 = a_0 + a_1\cos(\theta_n)a_2\sin(\theta_n) + a_3\cos(2\theta_n) + a_4\sin(2\theta_n) \quad \text{(B1)}$$

where R_0 is the average Earth-Sun distance and R_n is the Earth Sun distance on day d_n (0 for 1 January and 364 for 31 December). The coefficients a_0-a_4 are given in table C1, and

$$\theta_n \equiv 2\pi d_n / 365 \quad \text{(B2)}$$

R_n varies by about 3.4 % from minimum (perihelion, on about 3 January) to maximum (aphelion, on about July 5).

The solar zenith angle (SZA)

Solar radiation reaching the Earth's surface varies with time of the day, season and geographic location. All these variables are ascribed in one single parameter called the solar zenith angle (SZA) which is the angle between the local vertical direction and the direction of the center of the solar disk. That's why SZA is fundamental variable in the computations of radiation reaching the Earth's surface.

The general expression for SZA is,

$$\cos(SZA) = \sin(\delta)\sin(\phi) + \cos(\delta)\cos(\phi)\cos(t_n) \quad \text{(B3)}$$

where δ is the solar declination, ϕ is latitude and t_n is the local hour angle. Declination is the angle between the Sun's direction and equatorial plane, and varies between $+23.45^0$ (21 June) and -23.45^0 (21 December), crossing 0^0 at the spring and fall equinoxes. The solar declination is given by,

$$\delta = b_0 + b_1\cos(\theta_n) + b_2\sin(\theta_n) + b_3\cos(2\theta_n) \quad \text{(B4)}$$

$$+ b_4\sin(2\theta_n) + b_5\cos(3\theta_n) + b_6\sin(3\theta_n)$$

where d_n and θ_n is defined in Appendix B and the coefficients b_0-b_6 are given in table B1. Expression for the local hour angle (t_n) is,

$$t_h = \pi(GMT/12 - 1 + \psi/180) + EQT \tag{B5}$$

where ψ is the longitude and EQT is the equation of time which accounts for the nonuniformity of the apparent angular speed of the Sun in the sky. Values of EQT are computed with,

$$EQT = c_0 + c_1\cos(\theta_n) + c_2\sin(\theta_n) + c_3\cos(2\theta_n) + c_4\sin(2\theta_n) \tag{B6}$$

Coefficients c_0-c_4 are given in table B1.

i	a_i	b_i	c_i
0	1.000110	0.006918	0.000075
1	0.034221	-0.399912	0.001868
2	0.001280	0.070257	-0.032077
3	0.000719	-0.006758	-0.014615
4	0.000077	0.000907	-0.040849
5		-0.002697	
6		0.001480	

Table B1. *Coefficients for the Earth-Sun distance (a_i) and solar declination (b_i) from Madronich, 1993, and the equation of time (c_i) from Spencer, 1971.*

KNMI-PUBLICATIES, VERSCHENEN SEDERT 1995

Een overzicht van eerder verschenen publicaties, wordt verzoek toegezonden door de Bibliotheek van het KNMI, postbus 201, 3730 AE De Bilt, tel. 030 - 2 206 855, fax. 030 - 2 210 407; e-mail: biblioth@knmi.nl

▼ KNMI-PUBLICATIE MET NUMMER

150-28 Sneeuwdek in Nederland 1961-1990 / A.M.G. Klein Tank
176-S Stormenkalender: chronologisch overzicht van alle stormen (windkracht 8 en hoger) langs de Nederlandse kust voor het tijdvak 1990-1996 / [samenst. B. Zwart a.o.]
180a List of acronyms in environmental sciences : revised edition / [compiled by P. Geerders and M. Waterborg]
181b FM12 SYNOP . internationale en nationale regelgeving voor het coderen van de groepen 7wwW1W2 en 960ww; derde druk
183-1 Rainfall in New Guinea (Irian Jaya) / T.B. Ridder
183-2 Vergelijking van zware regens te Hollandia (Nieuw Guinea), thans Jayapura (Irian Jaya) met zware regens te De Bilt / T. B. Ridder
183-3 Verdamping in Nieuw-Guinea, vergelijking van gemeten hoeveelheden met berekende hoeveelheden / T.B. Ridder
183-4 Beschrijving van het klimaat te Merauke, Nieuw Guinea, in verband met de eventuele vestiging van een zoutwinningsbedrijf / T.B. Ridder a.o.
183-5 Overzicht van klimatologische en geofysische publikaties betreffende Nieuw-Guinea / T.B. Ridder
184a Inleiding tot de algemene meteorologie : studie-uitgave ; 2e druk / B. Zwart, A. Steenhuisen, m.m.v. H.J. Krijnen
185a Handleiding voor het gebruik van sectie 2 van de FM 13-X SHIP-code voor waarnemers op zee / KNMI; KLu; KM
186-I Rainfall generator for the Rhine Basin: single-site generation of weather variables by nearest-neighbour resampling / T. Brandsma a.o.
187 De wind in de rug: KNMI-weerman schaatst de Elfstedentocht / H. van Dorp

▼ TECHNISCH RAPPORT = TECHNICAL REPORT (TR)

168 Analyse van het seismische risico in Noord-Nederland / Th. de Crook a.o.
169 Evaluatie van neerslagprognoses van numerieke modellen voor de Belgische Ardennen in december 1993 / Erik van Meijgaard
170 DARR-94 / C.P.G. Lomme
171 EFEDA-91: documentation of measurements obtained by KNMI / W.A.A. Monna a.o.
172 Cloud lidar research at the Royal Netherlands Meteorological Institute KNMI2B2, version 2 cloud lidar analysis / A.Y. Fong a.o.
173 Measurement of the structure parameter of vertical wind-velocity in the atmospheric boundary layer / R. van der Ploeg
174 Report of the ASGASEX'94 workshop / ed. by W.A. Oost
175 Over slecht zicht, bewolking, windstoten en gladheid / J. Terpstra
176 Verification of the WAQUA/CSM-16 model for the winters 1992-93 and 1993-94 / J.W. de Vries
177 Nauwkeuriger nettostraling meten / M.K. van der Molen en W. Kohsiek
178 Neerslag in het stroomgebied van de Maas in januari 1995: waarnemingen en verificatie van modelprognoses / R.Jilderda a.o.
179 First field experience with 600PA phased array sodar / H. Klein Baltink
180 Een Kalman-correctieschema voor de wegdektemperatuurverwachtingen van het VAISALA-model / A. Jacobs
181 Calibration study of the K-Gill propeller vane / Marcel Bottema
182 Ontwikkeling van een spectraal UV-meetinstrument / Frank Helderman
183 Rainfall generator for the Rhine catchment : a feasibility study / T. Adri Buishand and Theo Brandsma
184 Parametrisatie van mooi-weer cumulus / M.C. van Zanten
185 Interim report on the KNMI contributions to the second phase of the AERO-project / Wiel Wauben, Paul Fortuin a.o.
186 Seismische analyse van de aardbevingen bij Middelstum (30 juli 1994) en Annen (16 augustus '94 en 31 januari '95) / [SO]
187 Analyse wenselijkheid overname RIVM-windmeetlokaties door KNMI / H. Benschop
188 Windsnelheidsmetingen op zeestations en kuststations: herleiding waarden windsnelheden naar 10-meter niveau / H. Benschop
189 On the KNMI calibration of net radiométers / W. Kohsiek
190 NEDWAM statistics over the period October 1994 - April 1995 / F.B. Koek
191 Description and verification of the HIRLAM trajectory model / E. de Bruijn
192 Tiltmeting : een alternatief voor waterpassing ? / H.W. Haak
193 Error modelling of scatterometer, in-situ and ECMWF model winds; a calibration refinement / Ad Stoffelen
194 KNMI contribution to the European project POPSICLE / Theo Brandsma a.o.
195 ECBILT · a coupled atmosphere ocean sea-ice model for climate predictability studies / R.J. Haarsma a.o.
196 Environmental and climatic consequences of aviation: final report of the KNMI contributions to the AERO-project / W. Wauben a.o.
197 Global radiation measurements in the operational KNMI meteorological network: effects of pollution and ventilation / F. Kuik
198 KALCORR: a kalman-correction model for real-time road surface temperature forecasting / A. Jacobs
199 Macroseismische waarnemingen Roswinkel 19-2-1997 / B. Dost e.a.
200 Operationele UV-metingen bij het KNMI / F. Kuik
201 Vergelijking van de Vaisala's HMP233 en HMP243 relatieve luchtvochtigheidsmeters / F. Kuik
202 Statistical guidance for the North Sea / Janet Wijngaard and Kees Kok
203 UV-intercomparison SUSPEN / Foeke Kuik and Wiel Wauben
204 Temperature corrections on radiation measurements using Modtran 3 / D.A. Bunskoek, A.C.A.P. van Lammeren and A.J. Feijt
205 Seismisch risico in Noord-Nederland / Th. De Crook, H.W. Haak en B. Dost
206 The HIRLAM-STAT-archive and its application programs / Albert Jacobs
207 Retrieval of aerosol properties from multispectral direct sun measurements / O.P. Hasekamp
208 The KNMI Garderen Experiment, micro-meteorological observations 1988-1989; instruments and data / F.C. Bosveld a.o.
209 CO2 in water and air during ASGAMAGE: concentration measurements and consensus data / Cor M.J. Jacobs, Gerard J. Kunz, Detlev Sprung a.o.
210 Elf jaar Cabauw-metingen / J.G. van der Vliet
211 Indices die de variabiliteit en de extremen van het klimaat beschrijven / E.J. Klok
212 First guess TAF-FGTAF: semi-automation in TAF production / Albert Jacobs
213 Zeer korte termijn bewolkingsverwachting met behulp van METCAST: een verificatie en beschrijving model-uitvoer / S.H. van der Veen
214 The implementation of two mixed-layer schemes in the HOPE ocean general circulation model / M. van Eijk
215 Stratosphere-troposphere exchange of ozone, diagnosed from an ECMWF ozone simulation experiment / Harm Luykx
216 Evaluatierapport Automatisering Visuele Waarnemingen . Ontwikkeling Meestsystemen / Wiel Wauben en Hans de Jongh
217 Verificatie TAF en TREND / Hans van Bruggen

▼ WETENSCHAPPELIJK RAPPORT = SCIENTIFIC REPORT (WR)

95-01 Transformation of precipitation time series for climate change impact studies / A.M.G. Klein Tank and T.A. Buishand
95-02 Internal variability of the ocean generated by a stochastic forcing / M.H.B. van Noordenburg
95-03 Applicability of weakly nonlinear theory for the planetary-scale flow / E.A. Kartashova
95-04 Changes in tropospheric NOx and O3 due to subsonic aircraft emissions / W.M.F. Wauben a.o.
95-05 Numerical studies on the Lorenz84 atmosphere model / L. Anastassiades
95-06 Regionalisation of meteorological parameters / W.C. de Rooy
95-07 Validation of the surface parametrization of HIRLAM using surface-based measurements and remote sensing data / A.F. Moene a.o.
95-08 Probabilities of climatic change : a pilot study / Wieger Fransen (ed.) a.o.
96-01 A new algorithm for total ozone retrieval from direct sun measurements with a filter instrument / W.M.F. Wauben
96-02 Chaos and coupling: a coupled atmosphere ocean-boxmodel for coupled behaviour studies / G. Zondervan
96-03 An acoustical array for subsonic signals / H.W. Haak
96-04 Transformation of wind in the coastal zone / V.N. Kudryavtsev a.o.
96-05 Simulations of the response of the ocean waves in the North Atlantic and North Sea to CO2 doubling in the atmosphere / K. Rider a.o.
96-06 Microbarograph systems for the infrasonic detection of nuclear explosions / H.W. Haak and G.J. de Wilde
96-07 An ozone climatology based on ozonesonde measurements / J.P.F. Fortuin
96-08 GOME validation at KNMI and collaborating institutes / ed. P Stammes a.o.
97-01 The adjoint of the WAM model / H. Hersbach
97-02 Optimal interpolation of partitions: a data assimilation scheme for NEDWAM-4; description and evaluation of the period November 1995 - October 1996 / A.Voorrips
97-03 SATVIEW: a semi-physical scatterometer algorithm / J.A.M. Janssen a.o.
97-04 GPS water vapour meteorology : status report / H. Derks a.o.
97-05 Climatological spinup of the ECBILT oceanmodel / Arie Kattenberg a.o.
97-06 Direct determination of the air-sea transfer velocity of CO2 during ASGAMAGE / J.C.M. Jacobs, W. Kohsiek and W.A. Oost
97-07 Scattering matrices of ice crystals / M. Hess, P. Stammes a.o.
97-08 Experiments with horizontal diffusion and advection in a nested fine mesh mesoscale model / E.I.F. de Bruijn
97-09 On the assimilation of ozone into an atmospheric model / E.Valur Hólm
98-01 Steady state analysis of a coupled atmosphere ocean-boxmodel / F.A. Bakker
98-02 The ASGAMAGE workshop, September 22-25, 1997 / ed. W.A. Oost
98-03 Experimenting with a similarity measure for atmospheric flows / R.A. Pasmanter and X.-L. Wang
98-04 Evaluation of a radio interferometry lightning positioning system / H.R.A. Wessels
98-05 Literature study of climate effects of contrails caused by aircraft emissions / V.E. Pultau